Electrochemistry of Soluble Methane Monooxygenase on a Modified Gold Electrode: Implications for Chemical Sensing in Natural Waters

by

Janet Duanping Chuang

B.S. Chemistry
University of California at Berkeley, 2001

Submitted to the Department of Civil and Environmental Engineering
in partial fulfillment of the requirements for the degree of

Master of Science in Civil and Environmental Engineering

at the

MASSACHUSETTS INSTITUTE OF TECHNOLOGY

June 2005

Author .....
Department of Civil and Environmental Engineering
March 1, 2005

Certified by ....
Harold F. Hemond
Professor of Civil and Environmental Engineering
Thesis Supervisor

Accepted by .....
Andrew J. Whittle
Chairman, Department Committee on Graduate Students

Electrochemistry of Soluble Methane Monooxygenase on a Modified Gold Electrode: Implications for Chemical Sensing in Natural Waters

by

Janet Duanping Chuang

Submitted to the Department of Civil and Environmental Engineering
on March 2, 2005, in partial fulfillment of the
requirements for the degree of
Master of Science in Civil and Environmental Engineering

Abstract

This work explored the possibility of using the soluble methane monooxygenase (MMO) enzyme, a three-component enzyme which catalyzes the oxygenation of methane and other substrates, to design a methane sensor for use in natural waters. Such a sensor would be useful for monitoring lake biogeochemistry, including the potential for lakes to be a source of methane into the atmosphere.

An op amp-based potentiostat was constructed, and a LabVIEW program was written to control the instrument and acquire data digitally. Cyclic voltammetry experiments were conducted with both acetonitrile, a liquid substrate, and the natural substrate methane. With the hydroxylase component of the enzyme (MMOH) adsorbed onto a peptide-modified gold electrode, the amount of charge transferred during a scan depended on both substrate and oxygen concentrations. This concentration dependence did not occur when MMOH was not present. In the case of methane, the kinetic limitations of partitioning between gas and liquid phases may have contributed to experimental scatter. These results raise the possibility that MMOH may be used without the other two components to generate a reproducible, concentration-dependent signal.

Signal strength was also dependent on the order in which high- and low-concentration trials were conducted. The hydroxylase may be able to store methane and oxygen in a hydrophobic cavity for later use, an observation that has both ecological and sensor-design implications.

Thesis Supervisor: Harold F. Hemond
Title: Professor of Civil and Environmental Engineering

Acknowledgments

The road towards this thesis hasn't always been smooth, and I am thankful for the many people who have helped me navigate the bumps (and at times, helped me find the road).

I am grateful to Harry Hemond for helping me find a new project to play with, and for providing feedback and guidance with a subject that isn't quite his specialty. I can't imagine many other advisors who would have done that, and I owe much to his imagination and tireless patience. Sheila Frankel and Phil Gschwend provided, among other things, inspiration and encouragement at key times. John MacFarlane was always available to pass on laboratory technique and wisdom. Tina Voelker allowed me to wander into her office and think out loud about why I was in grad school.

This project would not have gotten off the ground without the help of Matt Sazinsky, who provided me with protein samples and patient advice, and his advisor, Stephen Lippard. Yann Astier answered many preliminary questions about MMOH and electrodes. Kaity and Dana were always willing to explain the biology side of things to this non-biologist. Within the Hemond group, Joe was great company in the electronics lab, showing me around soldering and circuits and all things 6.002-related. Dave Senn offered his time to get me started on the Upper Mystic Lake project. Emilie was a great source of older-sister advice.

The Parsons Lab has been a great academic home, friendly and supportive, and I probably don't appreciate just how rare that is. Thanks to Vicki Murphy for all her help, and to Cynthia Stewart for dealing with me. Freddi-Jo Eisenberg doesn't know me, but her thesis (Ph.D, 2000) was an excellent model for this piece of writing.

I'm also grateful to Thetans for providing me with a home in the truest sense these past few weeks, and to the friends in Boston and elsewhere who have kept me mostly happy and sane. Thank you all for walking through the past couple of years with me; it's been a privilege and a blessing. Finally, thanks to my parents for their encouragement and unwavering support – anything I might accomplish or become is because of you.

This work was supported by a Presidential Fellowship, the EPA-funded Tufts-MIT Nutrient Project, and the William E. Leonhard Chair of Civil and Environmental Engineering.

Contents

List of Figures

List of Tables

Chapter 1

Introduction

The initial idea for this project was to develop a chemical sensor for methane, which would be part of a network of sensors used in conjunction with an underwater mass spectrometer. As it turns out, this project is a proof-of-concept one, illustrating that our particular approach towards sensor design is scientifically sound, if not yet practically useful.

Methane is an interesting chemical to monitor for several reasons. It is a useful indicator of redox reactions in a body of water; the presence of methane indicates that more favorable oxidants have already been used up. If methane is present in the deeper waters of a lake, for instance, then this water is not only anoxic, but also depleted of nitrate and sulfate, which play important roles in their respective element cycles. Methane is also a powerful greenhouse gas; while it is present in the atmosphere at far lower concentrations than carbon dioxide, it absorbs infrared radiation about 20 times more strongly, so that relatively small amounts can still have a significant impact on climate [25].

There are commercially available methane sensors that are designed for different uses than what we have in mind. We are looking for small, inexpensive sensors that can be mass-produced and networked; the sensor also needs to have a long lifetime, without requiring constant maintenance. The current *in situ* sensors are based on doped semiconductor surfaces, where the resistance changes upon adsorption of methane. These sensors are bulky and expensive, and have slow response times. Biological methane microelectrodes have also been developed; these are most useful for identifying concentration gradients over a short distance, such as the first few centimeters of a sediment bed. These are based on keeping a population of methanotrophs alive within the electrode; as the bacteria consume methane, they also consume oxygen, and it is actually the change in oxygen that

is measured [14]. However, the lifetime of these biosensors ranges from days to months, and the sensors must be exposed to methane once a week to maintain functionality, making them impractical for long-term undisturbed sampling.

Our approach is significantly different from either of these strategies. We explore the possibility of using a chemical sensing approach, which combines a molecular recognition event – a reaction that is specific to a certain molecule, for instance – with the production of some signal that can be measured, such as light intensity or electrical current. In this case, the methane monooxygenase (MMO) enzyme converts methane to methanol through a reaction that also consumes two electrons. By immobilizing the enzyme on an electrode surface, these electrons can come from the electrode, rather than from the cofactor that the enzyme uses in nature. The more methane is in solution, the more the MMO enzyme turns over; if two electrons are required every time the enzyme goes through its catalytic cycle, then ideally, the current measured at the electrode would be proportional to the concentration of methane in solution.

This thesis focuses on the questions of whether a MMO-modified electrode produces an electrical signal that is dependent on methane concentration in a reproducible way, and if so, over what concentration range. Chapter 2 presents background information about the MMO enzyme and immobilization techniques, while Chapter 3 introduces the technique of cyclic voltammetry. Experimental methods are described in Chapter 4. In Chapter 5, results from three categories of experiments are presented. The adsorption of the enzyme onto the electrode was examined first, followed by how signal changes with concentration for acetonitrile, an alternative substrate which is easier to work with; finally, the relationship between signal and methane concentration was investigated. Experiment-specific discussion accompanies the results, while more general observations are left to Chapter 6. The homemade instrumentation used to carry out the work is described in some detail in the Appendix.

Chapter 2

Background

2.1 Methane monooxygenase

The methane monooxygenase (MMO) enzyme is found in methanotrophs, a group of bacteria that are able to use methane as their sole source of carbon and energy [23]. It occurs in two forms, depending on the bioavailability of copper. In the presence of copper, particulate MMO (pMMO) is produced; this form is membrane-bound and difficult to study outside of the cell. Recently, progress has been made in isolating and characterizing the pMMO from *Methylococcus capsulatus* (Bath), but at present, not enough is known about its structure and function to make a pMMO-based sensor a practical goal [33].

Under low copper conditions, soluble MMO (sMMO) is produced instead; this form is easier to work with, and has been extensively studied in both *Methylosinus trichosporium* OB3b and *M. capsulatus* (Bath). The structure of sMMO is known, and the details of how its components interact and how its catalytic cycle proceeds are active areas of research; this information has been essential to our efforts at sensor design.

2.1.1 Structure

The soluble MMO from *M. capsulatus*, which was used in this project, consists of three components, as shown in Figure 2-1. The hydroxylase, MMOH, is a dimer – a compound with two identical units – each of which, in turn, is made up of α, β, and γ subunits. Each α subunit contains an active site with two iron atoms, where reaction with methane takes place. The reductase, MMOR, participates in electron transfer. It receives electrons from NADH (the reduced form of nicotinamide

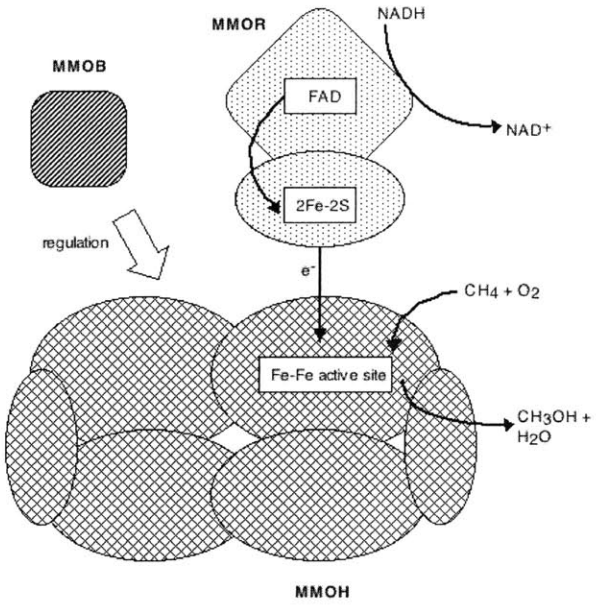

Figure 2-1: The hydroxylase, reductase, and coupling protein of soluble methane monooxygenase. Adapted from [40].

adenine dinucleotide, which participates in many cellular redox reactions), which are transferred stepwise to FAD (flavin adenine dinucleotide) and [2Fe-2S] cofactors, and finally to the active site in the hydroxylase. The third component, MMOB, is often described as a coupling protein; it appears to induce conformational changes that affect electron transfer and reactivity [40]. The MMOH component is by far the largest, with a molecular weight of 251 kDa; MMOR and MMOB are 39 and 16 kDa respectively. In the cell, the hydroxylase and coupling protein are present in approximately equal concentrations, while the concentration of the reductase is about one-tenth that of the other components. It is thought that MMOR can move easily from one enzyme molecule to another, so that one molecule of reductase can provide electrons to several hydroxylase active sites.

The crystal structure of MMOH provides insight about how oxygen and methane might access the active site. There is no direct access between the surface of the enzyme and the active site, which is buried below two long α-helices [46]. However, the iron atoms are located on one wall of a large hydrophobic cavity, and other hydrophobic pockets in MMOH could provide one access route; conformational changes could lead to the direct linkage of the hydrophobic areas. Also, conformational changes could separate the two α-helices, providing a shorter tunnel between the surface and active site.

The MMOH structure also reveals a long canyon between the α and β subunits, which could be a docking site for MMOB and MMOR. The component interactions will be discussed in more detail below.

2.1.2 Catalytic Cycle

The reaction catalyzed by MMO is the first step in the oxidation of methane, a sequence that produces formaldehyde, which can be incorporated into biomass, and finally carbon dioxide. The step catalyzed by MMO is the conversion of methane into methanol:

$$CH_4 + NADH + H^+ + O_2 \rightarrow CH_3OH + NAD^+ + H_2O$$

Several key features of the catalytic cycle, shown in Figure 2-2, are relevant to sensor work. From the resting state of the enzyme, in which both iron atoms are in the +III (ferric) oxidation state, a two-electron reduction proceeds which reduces each iron atom to the +II (ferrous) oxidation state. In nature, these electrons come from NADH; experiments have also been carried out in which the iron centers are chemically reduced. The next step is the incorporation of O_2, which proceeds quickly. The resulting complex then undergoes several internal transformations which do not involve additional reagents, leading to the formation of the Q intermediate. This unusual structure consists of iron atoms with a +IV oxidation state, arranged in a diamond core structure with two atoms of oxygen [35].

If no methane or alternative substrate is present, the step leading to Q is the rate-limiting step. It is not clear what happens next – whether the oxygen is released, and if the iron atoms return to the +III state – but in any case, the full catalytic cycle cannot proceed. If methane is present, however, it is incorporated into the active site once Q is generated. One of the oxygen atoms is inserted into a C-H bond, and then the oxidized product is released, returning the active site to its original +III state.

2.1.3 Component Interactions

One active area of MMO research focuses on how the three components of the enzyme work together to catalyze the reaction most efficiently. The component interactions are slightly different in protein from *M. capsulatus* and from *M. trichosporium*, but both will be discussed here to provide a general sense of what is known in this area.

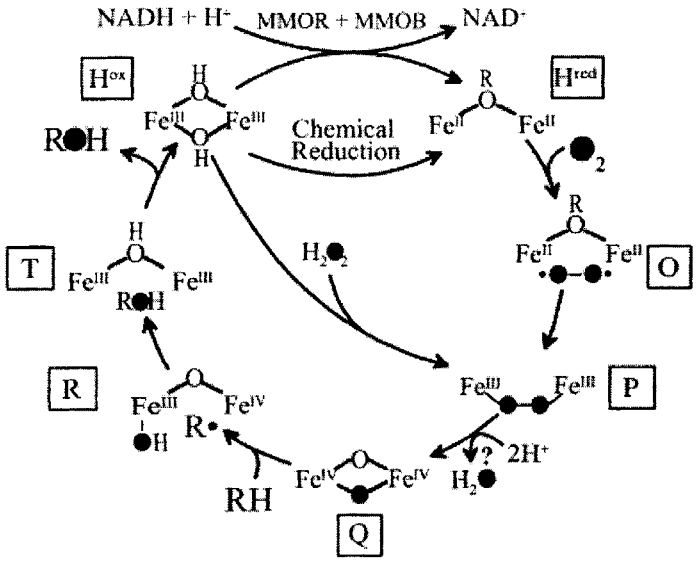

Figure 2-2: Catalytic cycle of soluble methane monooxygenase, from [35]. The darkened circles show the fate of oxygen atoms from dioxygen and hydrogen peroxide.

For maximum catalytic activity, all three components must be present. In the natural system, with NADH serving as the electron source, protein B must be present for turnover to occur in MMO from *M. capsulatus*. In MMO from *M. trichosporium*, protein B is not required, but it accelerates the rates of intermediate formation, and thus of the overall reaction [54, 36]. In both versions of the enzyme, MMOR and MMOB shift the redox potentials of the iron center, indicating that both components play a role in regulation of electron transfer.

Single turnover experiments, in which the hydroxylase is directly reduced by another chemical species instead of through the MMOB electron transfer chain, may be more relevant to this work. Work with *M. trichosporium* enzyme has shown that with hydroxylase alone, the yield of oxygenated product from a single-turnover reaction is about 40%. When MMOB is present, the yield increases to 80%, and when both MMOB and MMOR are present, the yield is close to unity [53]. For *M. capsulatus*, the presence of protein B at a molar ratio of 1.5 or greater (compared to MMOH) leads to increased yield, and also increases the overall rate of reaction [36]. The reductase does not have a significant effect on product yield or rate constant, suggesting that protein B might play a key role in facilitating turnover of MMOH on an electrode surface.

The interaction between hydroxylase and protein B has been probed in more detail in both *M. trichosporium* and *M. capsulatus*. Work on the *M. trichosporium* protein suggests that a key role of

MMOB is to allow the selective access of O_2 and CH_4 into the active site of MMOH by opening up a channel of the correct size, with the interaction stabilized by electrostatic forces between positively and negatively charged amino acids [11]. This hypothesis was tested by replacing the polar amino acids on MMOB with smaller, nonpolar ones to remove the electrostatic interaction that leads to size control; when this happened, reaction with methane was unaffected but reaction with larger substrates could proceed more easily [53].

Related work on the *M. capsulatus* protein focused on conformational changes over the entire hydroxylase molecule, rather than on the active site in particular. X-ray scattering data showed that the hydroxylase became longer and narrower upon complex formation; a model was proposed in which the binding of protein B leads to the conformational change, while the reductase plays a role in locking this position in place. The model further suggests that in the new conformation, the reductase is better able to interact with the active site, so that protein B plays a role in regulating electron transfer. A 1:2:2 (H:B:R) complex is formed, which is consistent with the dimeric nature of the hydroxylase [18]. It was also found that the presence of positively charged amino acids on the hydroxylase was essential to these interactions [5].

2.2 Immobilized Enzymes

It is often advantageous to immobilize enzymes on a solid support of some kind. For example, enzymes are very efficient catalysts for chemical synthesis, but if the enzyme is used in solution, the synthetic step must be followed by a difficult process of recovery. On the other hand, if the enzyme can be attached to glass or polymer beads which are used to pack a column, the same reaction can proceed, and removal of the enzyme for further use is much easier. This example illustrates a key concept in enzyme immobilization – the attachment must be strong enough to keep the enzyme on its solid support, yet not so strong that it disrupts the enzyme so that it is no longer functional.

One simple approach to enzyme immobilization is that of physical entrapment. This technique can be used in sensors; for example, a urea electrode can be constructed by immobilizing the enzyme urease, which converts urea to ammonia and carbon dioxide, over an ammonia electrode. In this case, the enzyme is sandwiched between a gas-permeable membrane, which allows ammonia to pass through to the electrode, and a dialysis membrane which selects for urea; neither membrane allows the enzyme to pass through [44]. A similar sensor can be made for glucose, in which the glucose

oxidase enzyme is entrapped between two membranes over an amperometric probe. The reaction of glucose with oxygen produces H_2O_2, which is measured directly by the probe. The proximity of glucose oxidase to the probe allows signal to be measured without requiring catalytic cycling of the enzyme to amplify the signal [49].

A variation on physical immobilization between membranes is to trap the enzyme within a cross-linked polymer such as polyacrylamide. The resulting structure is sufficient to keep the large enzyme molecule in place, but allows for the passage of small substrate molecules. Enzymes can also be immobilized through covalent bonding to a solid support, which has the advantage of being a more permanent means of attachment. However, it can be difficult to preserve the activity of the enzyme in this case, since unlike with entrapment within a polymer, the enzyme itself is being modified [38, 31].

As a 1983 review article pointed out,

> In principle, virtually any compound can be assayed by an enzyme electrode composed of a suitable electrochemical probe and an immobilized enzyme or a combination of enzymes acting in sequence [31].

However, the development of the glucose electrode marked the first time this principle became a commercial reality. One reason for its success has to do simply with characteristics of the glucose oxidase enzyme. The enzyme is stable, able to withstand more variation in pH, ionic strength, and temperature than most enzymes. Glucose oxidase is also easy to obtain, and while it is produced by fungi, the concentrations found in human blood fall within the range in which the enzyme is most effective [52]. Also, the need for home test kits for diabetic patients provided an economic driving force for development of a glucose-sensing device.

The use of glucose oxidase to detect blood glucose levels was already routine in clinical settings, with protocols which generally measured the hydrogen peroxide produced by the enzyme:

$$\text{glucose} + O_2 \rightarrow \text{gluconolactone} + H_2O_2$$

In the natural reaction, glucose is oxidized to gluconolactone, while the FAD cofactor of the enzyme is reduced to $FADH_2$. These electrons were then transferred to oxygen, leading to the production of H_2O_2 and the return of FAD to its resting, oxidized state. This situation is shown in the left-hand side of Figure 2-3.

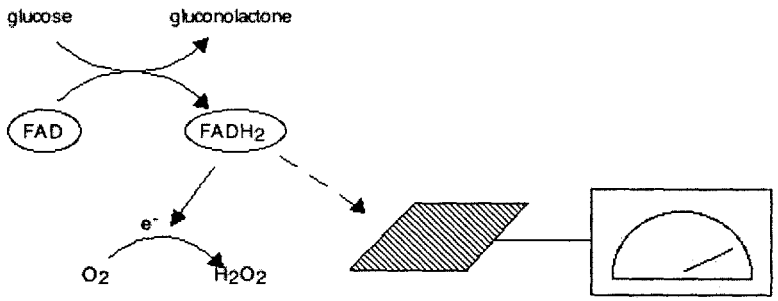

Figure 2-3: Schematic representation of glucose sensor. Electrons produced by the oxidation of glucose are transferred to an electrode (dashed arrow), rather than to oxygen (solid arrow).

For sensor work, it was desirable to have an alternative detection scheme not based on oxygen, since changes in oxygen level, as well as glucose concentration, could affect the signal. An initial strategy was to introduce a ferrocene derivative as a mediator. Ferrocenes – "sandwich" compounds with an iron atom between two parallel C_5H_5 rings, which can be modified by introducing substituents onto the rings – are electrochemically well-behaved, with Fe^{III}/Fe^{II} redox potentials that can be shifted by ring substitution. 1,1'-dimethylferrocene was found to be an effective mediator, and was immobilized along with glucose oxidase onto a graphite electrode. The oxidized form (ferricinium ion) accepts electrons from $FADH_2$ in place of oxygen, and then transfers these electrons to the electrode, so that it acts as a shuttle for electrons [12].

This initial work has been followed by the development of various strategies for immobilizing the glucose oxidase enzyme:

- Ferrocene-modified pyrrole units were codeposited onto the electrode surface along with the enzyme. Polypyrrole is a conducting polymer, and ferrocene units were attached to pyrrole before polymerization to aid in electron transfer. The enzyme and ferrocene are immobilized more strongly, leading to slower reaction rates and lower catalytic efficiency; this system is otherwise similar to that described above [16].

- An interesting extension of this idea involved the polymerization of silicon-based units, some of which are modified with ferrocene. The resulting chains are relatively free to rotate, leading to more effective contact between ferrocene and the FAD cofactor [22].

- The FAD cofactor was removed from the enzyme and modified with ferrocene, and the enzyme

was then reconstituted. The modified enzyme was then adsorbed onto a gold foil electrode that had been coated with a cystamine monolayer. The Michaelis-Menten constants were similar to those for a system with unmodified enzyme and a ferrocene-based mediator, suggesting that effective electrical contact was achieved [45].

- This concept was taken one step further by coating a gold electrode with a monolayer of chain molecules; these contain a quinoline derivative, which is effective in electron transfer, and end with a FAD unit. The FAD-stripped enzyme was then reconstituted onto this modified electrical surface, resulting in an electron transfer rate close to that found in nature. In this system, electrons are transferred sequentially from the FAD cofactor to the quinoline, and finally to the electrode [29].

While some of these later approaches are more sophisticated and probably more efficient, the original strategy, of immobilizing glucose oxidase and ferrocene mediator onto a carbon electrode, has successfully been developed into a commercial product. In the Exactech glucose sensor, single-use glucose electrodes consist of a mixture of enzyme and mediator in a carbon paste; these are used with a meter containing the electronics and display [52]. This sensor represents a significant advance from the older generation of home-use glucose sensors, in which the color change produced by H_2O_2 is compared by eye to a reference chart. The glucose electrode story might also be taken as an argument for simplicity; while the strategy used in the commercial sensor may not be as elegant as some of the approaches developed more recently, it is nonetheless one that gives reproducible results, and does so relatively inexpensively. Since these are the characteristics we are looking for in an *in situ* methane sensor, the development of glucose-sensing devices provides a valuable set of guiding principles in the effort to develop a similar product for methane.

2.3 Adsorption of MMO

In this project, immobilization of the MMO hydroxylase was achieved by adsorbing it onto a gold electrode that had been modified with a coating of peptide. This strategy was a natural extension of a series of studies which investigated the electrochemistry of small electron transfer proteins at similarly modified electrodes.

The goal of this area of research is to imitate, at an electrode surface, the interaction a protein would have with its natural redox partner. However, electron-transfer reactions often involve a

temporary rearrangement of the bonds closest to the metal center, in what is termed an inner-sphere reaction. If this rearrangement happened at an electrode surface, it might not be reversible, leading to loss of protein activity [3]. As is the case for all enzyme immobilization techniques, adsorption must hold the enzyme strongly enough to attach it to the surface, while not be so strong that denaturation occurs. In general, the protein also needs to be bound to the electrode surface in a particular orientation to make electron transfer possible, since the active site is usually buried in the protein [17].

Initial work in this area showed that for horse-heart cytochrome *c*, electron transfer was facilitated by surface modifiers that could interact effectively with both the protein and electrode. The amino acid cysteine fulfills both criteria; the thiol group forms a S-Au bond to the electrode, while the amine and carboxylate groups interact with charged amino acids around the binding site of cytochrome *c* [15].

Next, the effects of coating the gold electrode with cysteine-containing peptides was investigated. This work focused on four small redox proteins, including cytochrome *c*, and showed how the surface modifier could be "tuned" for the particular protein by varying the peptide chosen. For for a given peptide, changing the pH or ionic strength of the solution had an effect as well [7]. The role of the peptide layer is twofold: to provide a set of electrostatic interactions similar to that of the protein's natural redox partner, and to prevent degradation of the protein at the electrode surface. The use of short peptides, rather than lone cysteine amino acids, helps to achieve both goals; more specific electrostatic interactions can be tailored, and the peptides are flexible enough to accomodate a range of protein conformations. In essence, the peptide layer "cushions" the protein as the protein approaches the electrode surface.

The strategy of using a peptide to modify a gold electrode surface was first used for MMO in a study that determined the redox potentials of the iron centers, work that had been previously done using mediators in redox titrations. This work was the first to carry out direct electrochemistry of the iron centers of MMOH. A hexapeptide, Lys-Cys-Thr-Cys-Cys-Ala, was used as the modifier. The cysteine residues bind to the gold surface, while the lysine provides the positive charge that appears to be necessary for electron transfer between the hydroxylase and electrode surface. This observation may be in conflict with component interaction studies of *M. capsulatus*, which suggest that positively charged amino acids on MMOH are necessary for the interactions with MMOB and MMOR that lead to conformational change and effective electron transfer [5]. (If both the peptide and MMOH are positively charged, then it seems that a small negatively charged species would

also be necessary for effective electrostatic interaction.)

In any case, the fact that the hydroxylase could undergo redox reactions at an electrode surface without being denatured marked a significant advance. However, it was not possible to elucidate the nature of the peptide-protein interaction in any further detail; the authors simply stated that "an electrode modified with peptides provides a more congenial surface to attract an enzyme" [30]. Recent work on other proteins has clarified the role of the peptide layer. In addition to preventing denaturation of the enzyme at the bare gold surface, it also serves to keep the enzyme in a particular orientation for which electron transfer is most effective [9, 41]. For example, if the gold surface is covered by a layer of peptide, the enzyme cannot form S-Au bonds via its own cysteine residues which might hold the enzyme in an unfavorable orientation.

After the direct electrochemistry of MMOH was observed, continued work led to a key follow-up result: not only could the hydroxylase accept electrons from the electrode, as had been seen previously, but production of methanol was seen as well [4]. When acetonitrile was used as a substrate in place of methane, the oxygenation reaction was also observed. However, the formation of product from either substrate only proceeded when MMOB, optimally in a 2:1 ratio to MMOH, and catalase were both present. The requirement for catalase is a somewhat surprising one, indicating that the electrochemical system is producing hydrogen peroxide which deactivates the enzyme or otherwise prevents the oxygenation of methane. In the natural system, with all three components present and with NADH serving as the electron source, H_2O_2 does not appear to be produced. There is some mention in the literature of a "peroxide shunt" in which H_2O_2 catalyzes the oxygenation reaction by serving as a source of both electrons and oxygen, a different role altogether [2, 28].

The general idea for this project, then, was to combine the techniques developed in these works with our unique motivation. The work that focused on the direct electrochemistry of MMO provided a particularly useful springboard, since the techniques used to probe the iron center and component behavior could also be used to investigate whether MMO could be the basis of a methane sensor.

Chapter 3

Cyclic Voltammetry

3.1 General Case

Cyclic voltammetry is a versatile, widely used technique in many areas of chemistry, including that of catalytic reactions carried out by adsorbed species. It is most useful as a qualitative probe which quickly provides a wealth of information about redox reactions, such as the number of electrons transferred, the redox potential(s), and whether the reaction is reversible. For precise, quantitative results, other electrochemical methods are preferred [32], but cyclic voltammetry can still provide a useful first estimate.

The technique consists of applying a varying voltage to a system, and measuring the current response. More specifically, the applied voltage begins at a potential at which current is expected to be negligible, called the starting potential. The voltage decreases at a constant rate until the switching potential is reached, and then returns to the starting potential at the same rate; this is shown in Figure 3-1. These two segments make up one complete scan, returning the system to its original state.

The ferricyanide ion, $[Fe(CN)_6]^{3-}$, is well-behaved electrochemically and provides a simple example; its cyclic voltammogram is shown in Figure 3-2. At the starting potential, the iron is in the +III oxidation state. When the potential is sufficiently low, electron transfer from the electrode to the iron atom will be thermodynamically favorable, and the iron will be reduced to the +II state. At the end of the forward scan, as the first segment is called, $[Fe(CN)_6]^{4-}$ is present near the electrode surface. Finally, as the voltage is increased during the reverse scan, this species is oxidized back to Fe(III).

The shape of cyclic voltammetry curves is dependent on many factors, and analytical solutions

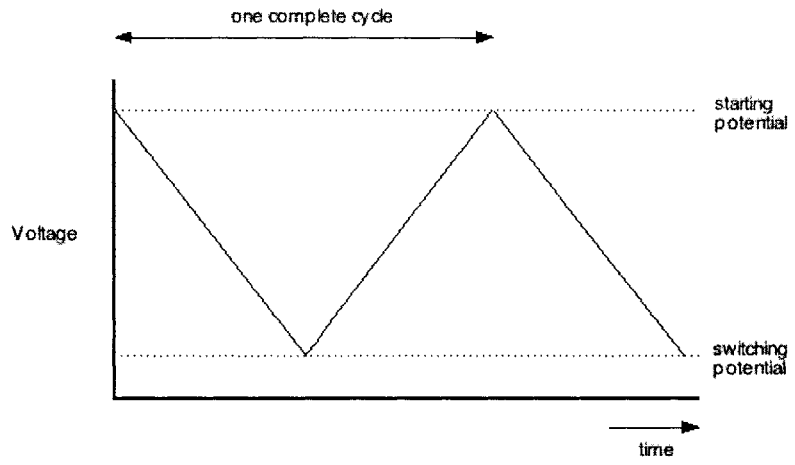

Figure 3-1: Applied voltage as a function of time

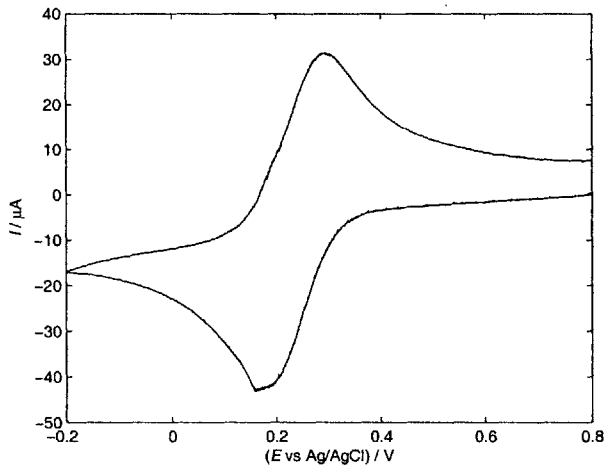

Figure 3-2: Cyclic voltammogram of ferricyanide, $[Fe(CN)_6]^{3-}$, showing current (I) as a function of applied potential (E).

are quite complicated [42]. An excellent, detailed introduction can be found in sources such as [6] and [47]. However, a general understanding can be developed by considering the physical and chemical processes in a conceptual, less quantitative manner.

The current response of a redox-active system depends on (1) the thermodynamics of the redox couple, (2) electron-transfer kinetics, and (3) mass transfer processes. Other complications, related to chemical reactions following the electrochemical step, will not be considered here. For the simplest case, we will assume that electron transfer is fast enough that the current is not kinetically limited; in this case, the reaction is said to be reversible.

The Nernst equation describes how the relative concentrations of oxidized and reduced species depend on the potential:

$$E = E^\circ + \frac{0.059}{n} \log \frac{[\text{Ox}]}{[\text{Red}]} \tag{3.1}$$

In this equation, [Ox] and [Red] are the concentrations of the oxidized and reduced species, and n is the number of electrons transferred in the reaction. The constant E° is the reduction potential, the potential at which concentrations of the oxidized and reduced species are equal, and E is the actual potential. Since $n = 1$ for ferricyanide, rearrangement leads to

$$\frac{[\text{Ox}]}{[\text{Red}]} = 10^{\frac{E-E^\circ}{0.059}} \tag{3.2}$$

As the potential is increased past E°, the [Ox]/[Red] ratio increases sharply. This increase is reflected in the cyclic voltammogram up to a point, and then the current falls off as voltage continues to increase. To explain this effect, transport effects must be considered as well. A simpler case, in which the potential is held at a constant level instead of changing with time, can be considered first. In the ferricyanide example, we consider an applied voltage low enough to essentially reduce all Fe(III) to Fe(II) at the electrode surface. In terms of Equation 3.2, when E is low enough compared to E°, the ratio of [Ox]/[Red] is close to zero, and [Ox] is negligible.

Mathematically, this can be treated as a boundary condition of $C = 0$ at $x = 0$, where x is the distance from the electrode surface and C refers to concentration of the oxidized species. This condition is imposed beginning at $t = 0$. For $t \geq 0$, the concentration profile is given by the complementary error function:

$$C(x) = C^*[1 - \text{erfc}(\frac{x}{2\sqrt{Dt}})] \tag{3.3}$$

where C^* is the concentration in bulk solution and D is the molecular diffusion coefficient; Figure

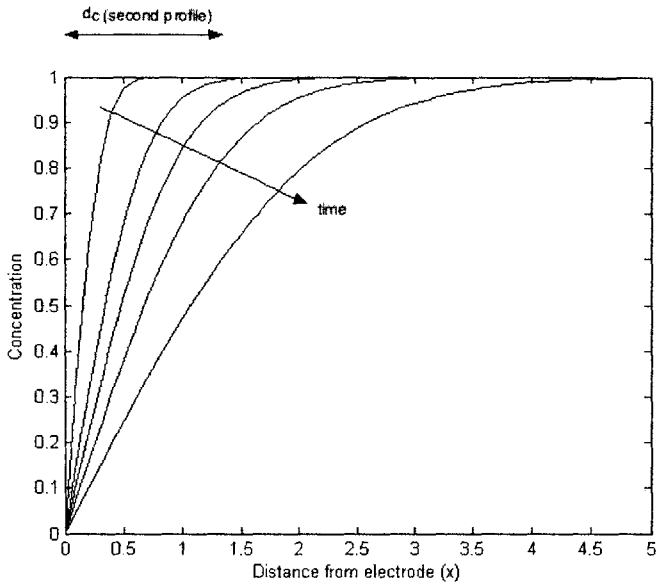

Figure 3-3: Concentration profile as a function of time, for conditions described in the text. Values of C are relative to C^*, while values of x are arbitrary.

3-3 shows how the profile evolves with time. The width of the concentration boundary layer, defined as the region in which C is less than $0.995C^*$, is given by $\delta_c = 4\sqrt{Dt}$.

We are interested in how current evolves with time in this situation. Since current is a flux of charge, and since each molecule of Fe(III) that contacts the electrode surface is reduced to Fe(II) under the given boundary condition, this is the same as considering how the concentration gradient, evaluated at $x = 0$, evolves with time. The relationship between current and concentration gradient is an expression of Fick's first law:

$$i = nFAD(\frac{\partial C}{\partial x})_{x=0} = K(\frac{\partial C}{\partial x})_{x=0} \tag{3.4}$$

where i is current, F is Faraday's constant, and A is the electrode surface area (which is different from the geometric area, due to surface roughness, but may be difficult to estimate).

To understand how $\partial C/\partial x$ changes with time, an intuitive approach is sufficient. The erfc function is self-similar; if the concentration profile at any time t is normalized by δ_c at that time, the result is the same for all values of t. As a result, since $\delta_c \sim \sqrt{Dt}$, $\partial C/\partial x \sim 1/\sqrt{Dt}$. This is in agreement with the solution obtained analytically:

$$(\frac{\partial C}{\partial x})_{x=0,t} = \frac{C^*}{\sqrt{\pi Dt}} \tag{3.5}$$

When the potential is varied linearly, the $t^{-1/2}$ dependence of current still holds. In fact, once the peak current has been reached, the current is solely controlled by transport rather than by thermodynamics, and is independent of potential. From this point, the decay with time will actually be the same if the scan is stopped and no voltage is applied [32]. A more descriptive explanation of the decay may also be useful: as the thickness of the depleted layer increases, the time needed for a reactant molecule to diffuse across this layer also increases. As a result, the rate at which reactant molecules reach the surface decreases, causing the current to decrease as well [37].

3.2 Variations

The cyclic voltammetry of ferricyanide, described above, provides a useful starting point for the development of basic theory (and, as we found, for the development of homemade instrumentation). It involves a reversible one-electron transfer, with a species that is freely diffusing in solution, and the redox reaction is not followed by subsequent irreversible chemical reactions. However, cyclic voltammetry is most widely used to investigate systems that do not fit this description in some way.

3.2.1 Reversibility

A quasi-reversible or irreversible reaction is one that is limited by electron-transfer (ET) kinetics, so that the Nernst equation does not adequately explain the relative concentrations of oxidized and reduced species. In the trivial limiting case, when the rate constant for electron transfer is zero, the ratio of [Ox]/[Red] will not change at all with potential, and the Nernst equation has no predictive power.

The reversibility of a given reaction depends on the rate of electron transfer relative to the scan rate, which is the rate at which the voltage is changed. For a series of scans at the same scan rate, as the ET rate constant is decreased, the peak current is observed to shift in the direction of the scan. This is because as the reaction kinetics slow down, it takes the system a longer time to respond to a given applied voltage [43].

For a reversible reaction, the ratio of the forward and reverse peak currents is unity, and the

peaks are spaced by $(0.059/n)$ V. The peak current is given by the Randles-Sevcik equation:

$$i_p = (2.69 \times 10^5) n^{3/2} A D^{1/2} C v^{1/2} \tag{3.6}$$

Most notably, the peak current increases linearly with concentration and with the square root of the scan rate v [32]. For irreversible reactions, however, these equations are not applicable.

The rate of an electron-transfer reaction at an electrode is, to some extent, predictable for a given molecule. If a certain molecule has slow ET rate constants in nature, it is likely to undergo slow electron transfer at an electrode surface as well. ET rate constants can be estimated using a model known as Marcus Theory:

$$k_{et} = (\frac{4\pi^2}{h}) T_{DA}^2 (\mathrm{FC}) \tag{3.7}$$

where h is Planck's constant.

In this expression, T_{DA}^2 is a measure of how well the wavefunctions of the donor and acceptor overlap, and thus how likely an electron is to tunnel between the two. It depends on the distance between donor and acceptor, as well as the medium between the two:

$$T_{DA}^2 = (T_{DA}^2)^\circ \exp(-\beta(R - R_\circ)) \tag{3.8}$$

R is the distance between donor and acceptor, while $R_\circ$ is the Van der Waals contact distance, the smallest possible distance between the two. The overlap is optimal at this distance, and this maximum value is expressed by $(T_{DA}^2)^\circ$. As the distance increases, the rate constant decreases exponentially. The constant β adjusts for the medium, accounting for how tunneling is least likely through a vacuum, and most likely through a network of covalent bonds.

The FC part of the expression is used to relate both the thermodynamic driving force ($\Delta G_\circ$, how energetically favorable is it to transfer the electron) and the reorganization energy (λ, how much the donor or acceptor has to change its physical arrangement) to the overall ET constant:

$$\mathrm{FC} = \frac{1}{\sqrt{4\pi\lambda k_B T}} \exp[\frac{-(-\Delta G_\circ - \lambda)^2}{4\lambda k_B T}] \tag{3.9}$$

where k_B is the Boltzmann constant and T is absolute temperature. The effects of $\Delta G_\circ$ and λ are at the heart of Marcus Theory. Specifically, this predicts that as the driving force is increased, the ET rate also increases to a maximum; past this point, rate actually decreases with increased driving force [34].

This model was developed to explain electron transfer rates between two molecules, but the concepts are relatively applicable to ET at an electrode surface as well. In this case, the electron is tunneling between states on the electrode and the reactant molecule; the effects of distance and the intervening medium are clearly still important. The effects of λ are the same; the ET rate constant decreases as greater reorganization of the reactant molecule is required. In the electrode case, though, instead of having a fixed ΔG_o, the driving force changes over the course of a scan. (The change in applied voltage shifts the energy states of the metal, making ET more or less favorable from an energetic standpoint.) There is also a theoretical difference: the inverted region, in which $-\Delta G_o > \lambda$ and the reaction actually slows down, does not occur with electron transfer at a metal electrode [6].

3.2.2 Surface Adsorption

Instead of a reactant molecule that is in solution, diffusing to and from the electrode, the redox-active molecules might be adsorbed onto the surface of the electrode. An interesting undergraduate experiment, presented in the *Journal of Chemical Education* [39], will be described here in some detail because it is conceptually similar to much of the MMO/methane work.

In this experiment, a graphite pencil is used as the working electrode; when it is scanned from +0.6 to +0.1 V versus the Ag/AgCl reference electrode, very little current flow is observed ($< 1\mu$A at a scan rate of $v = 100$ mV/s).

The electrode was then dipped in a 5 mM solution of phosphomolybdic acid, $H_3PMo_{12}O_{40}$, for 10 s. A scan was recorded from +0.6 to –0.1 V at 100 mV/s. This signal, shown in Figure 3-4, is dramatically different from that taken before adsorption; three large (close to 10 μA) peaks are seen, corresponding to successive two-electron transfer steps.

The total charge transferred, found by integrating the current with respect to time, can be used to estimate how densely the surface is covered with adsorbed molecules:

$$Q = nFA\Gamma \tag{3.10}$$

where Q is the charge and Γ is the surface coverage, expressed in moles/area.

The surface coverage can also be estimated by measuring the peak current at various scan rates:

$$i_p = \frac{n^2F^2vA\Gamma}{4RT} \tag{3.11}$$

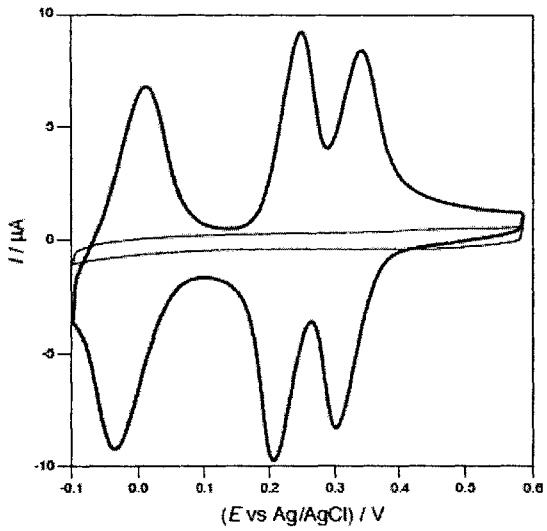

Figure 3-4: Scans of a graphite pencil electrode at 100 mV/s. The strong, distinct peaks seen after adsorption of phosphomolybdic acid (thick lines) are a marked contrast from the essentially flat signal seen before adsorption (thin lines). From [39].

where R is the ideal gas constant. In this experiment, the Γ values found by these two methods agreed to within 10%. By approximating the polyoxometalate molecule as a square of a known size, a theoretical surface coverage was also calculated. This value was also close to the experimental ones, indicating that the electrode was covered with a monolayer of $PMo_{12}O_{40}^{3-}$.

Finally, the modified electrode was used to catalyze the reduction of hydrogen peroxide, which does not proceed readily on bare graphite. When H_2O_2 was added to solution, the signal around 0.1–0.2 V shifted towards more negative currents, as shown in Figure 3-5. The reduction current increased significantly, while the oxidation current decreased. This is a result of catalytic behavior; the reduced species, $PMo_{12}O_{40}^{7-}$, cannot be oxidized electrochemically if it reacts with H_2O_2 first. Meanwhile, this produces more $PMo_{12}O_{40}^{5-}$, which can be electrochemically reduced again.

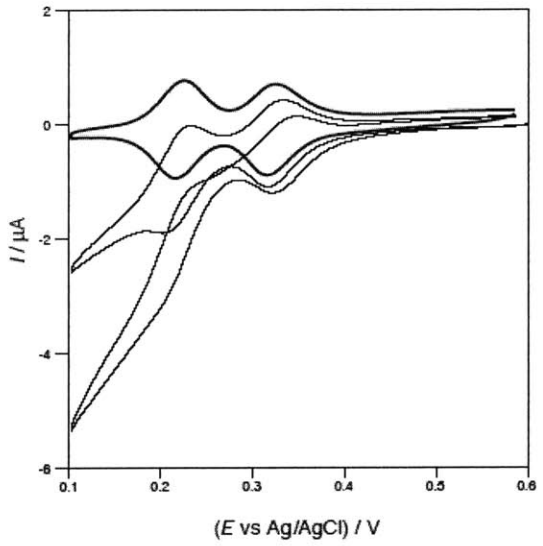

Figure 3-5: Catalysis carried out by a surface-adsorbed species. The two more positive peaks from Figure 3-4 are shown here, before the addition of hydrogen peroxide (thick lines) and after the addition of 150 and 300 mM H_2O_2 (thin lines); scans were taken at 10 mV/s. From [39].

Chapter 4

Methods

Materials

Biomaterials Solutions of MMOH and MMOB (70 μM MMOH and 1.6 mM MMOB, in 5% glycerol) from *M. capsulatus* (Bath) were obtained from the laboratory of Stephen Lippard in the MIT Chemistry Department, and were stored at -80°C. The MMOH had been frozen into beads, while the MMOB was present as a small aliquot. The Lys-Cys-Thr-Cys-Cys-Ala hexapeptide was synthesized and purified by reverse phase HPLC by the MIT Biopolymers Laboratory; the purified solid was stored at 4°C. MOPS buffer (25 mM, pH 7.0) was made in milli-Q ultrapure water (18.2 $M\Omega \cdot cm$ resistivity) and adjusted to neutral pH with NaOH. 1 mM peptide solutions were made in this buffer, divided into 0.2 mL aliquots, and stored at -20°C.

Electrochemical Setup The electrochemical cell and electrodes were obtained from Bioanalytical. The basic cell consists of a small, cylindrical glass container and a Teflon lid that accomodates the electrodes; the working, reference, and counter electrodes are placed in the holes of the lid. For peptide and protein work, a small-volume cell is necessary. This cell has a conical bottom and is sealed with a Vycor frit; the working and counter electrodes are placed inside, and then the small-volume cell is placed in the larger cell. The reference electrode remains outside the small-volume cell. The solution of interest is contained in the small-volume cell, while the outer cell contains background electrolyte at the same concentration, but no redox-active species.

The working electrode contains a plug of gold 3mm in diameter, encased in a plastic electrode body. A platinum wire electrode was used as the counter electrode, and an Ag/AgCl electrode was used as the reference; all potentials reported are relative to Ag/AgCl.

The potentiostat system includes the actual circuit, which was built on a breadboard and driven by a power supply, and the LabVIEW-equipped computer used to control the instrument and record data. The potentiostat circuit and LabVIEW code are described in detail in the Appendix.

Procedure

Electrode Cleaning The working electrode was cleaned before each day's experiments, using an electrode cleaning kit (Bioanalytical). The electrode was rinsed briefly with distilled water and methanol. A few drops of a 1 μm diamond slurry were applied to a wetted nylon cleaning disk, and a figure-eight pattern was traced out with the electrode for about a minute. After rinsing to remove residual particles, the cleaning process was repeated using an alumina suspension on a microcloth disk. The electrode was then sonicated for 5 minutes in a small amount of distilled water.

The Ag/AgCl electrode was stored in 3 M NaCl to prevent the frit from drying out; it required no other maintenance. The Pt electrode was occasionally wiped with a methanol-soaked Kimwipe, but in general, rinsing with milli-Q water was sufficient.

Preliminary Steps An 0.2 mL aliquot of peptide solution was thawed and then transferred to the small-volume cell. The newly cleaned working electrode was placed in the solution, along with the counter electrode. The electrode was cycled 10 times from +0.7 to –0.7 V at a scan rate of 100 mV/s. After peptide loading was complete, the electrode was rinsed with milli-Q water, but not wiped dry.

Meanwhile, a small amount of MMOH was thawed (two medium-sized beads provide an adequate amount of protein). The beads were removed from the storage container with forceps, and care was taken to return the rest of the beads to the -80°C freezer as quickly as possible. From the thawed solution, 120 μL was removed and diluted 1:1 with MOPS buffer, and 0.2 mL of the resulting 35 μM solution was transferred to the small-volume cell. The electrode was then cycled 10 times from 0 to –0.6 V at 5 mV/s in order to adsorb the protein onto the peptide-modified electrode.

Acetonitrile Experiments Acetonitrile (Mallinckrodt, HPLC grade) was diluted by a factor of 10^4 using milli-Q water. 0.2 mL of MOPS buffer was added to the small-volume cell, and the solution was degassed (except where noted) by bubbling a slow stream of argon through the solution for 3 minutes. The diluted CH_3CN solution was added in 3 or 5 μL aliquots using a microsyringe,

and briefly stirred by replacing the working electrode in the solution several times. After each addition of acetonitrile, the electrode was cycled once from 0 to –0.6 V at 50 mV/s. The solution was not further degassed after each addition.

Methane Experiments Gas mixtures were made in 30-mL wetted glass syringes fitted with 3-way stopcocks. Gas cylinders were fitted with regulators and septa, and gas lines were flushed by inserting the syringe needle into the septum and allowing gas to flow briefly. Syringes were filled by inserting the needle into the septum and allowing the pressurized gas to push back the barrel of the syringe. Oxygen was obtained from a small cylinder within a welding apparatus; in this case, the needle was inserted directly into the nozzle. The syringe was filled with 0–2 mL of oxygen and 0–8 mL of methane, and then the total volume was brought to 20 mL using helium. Except for oxygen, which was from Wesco and of unknown purity, all gases were laboratory-grade and obtained from BOC or Airgas.

For each scan, a fresh 0.2 mL of MOPS buffer was transferred to the small-volume cell. The appropriate gas mixture was bubbled slowly through the solution; in general, 15 mL of gas was bubbled into the solution over about a minute, and the remaining 5 mL was used to blanket the solution. The working and counter electrode were then placed in the solution, and scans were recorded from 0 to –0.6 V at various scan rates.

Chapter 5

Results

5.1 Peptide and Protein Loading

5.1.1 Peptide Signals

When the electrode was placed in a solution of peptide and cycled at reducing potentials, following the procedure described in [30], the signal decreased with each subsequent scan (Figure 5-1). The reason for this is not entirely clear. One possibility is that the peptide is not the electroactive species. There could be some other species in solution that is redox-active, and as the peptide covers more of the electrode surface, there is effectively less surface area for the redox reaction to occur. The only other species present in solution is 3-(N-morpholino)propanesulfonic acid, or MOPS, which acts as a buffer. It has a SO_3H group, which is weakly acidic and dissociates to form the conjugate base; it is possible, but unlikely, that the sulfur could also undergo redox transitions.

For comparison, the clean electrode was cycled under the same conditions in a solution that contained MOPS only. The results are shown in Figure 5-2. There is a reduction peak around –0.3 V and an oxidation peak around +0.5 V applied voltage. Both the reduction and oxidation signals shift to more positive values as the scans continue, unlike with the peptide, where signal strength decreases with successive scans. The peaks could be due to oxygen in solution. In an unbuffered solution at pH 7, oxygen reduction occurs around –0.1 V [26]; this solution is at pH 7 but buffered, so assigning the peaks to oxygen seems reasonable.

These figures also suggest that cyclic voltammetry signals are not necessarily additive. The peptide scans do not appear to be a superposition of some other signal on top of the MOPS-only one. In this case, the attachment of peptide molecules to the electrode may be preventing oxygen

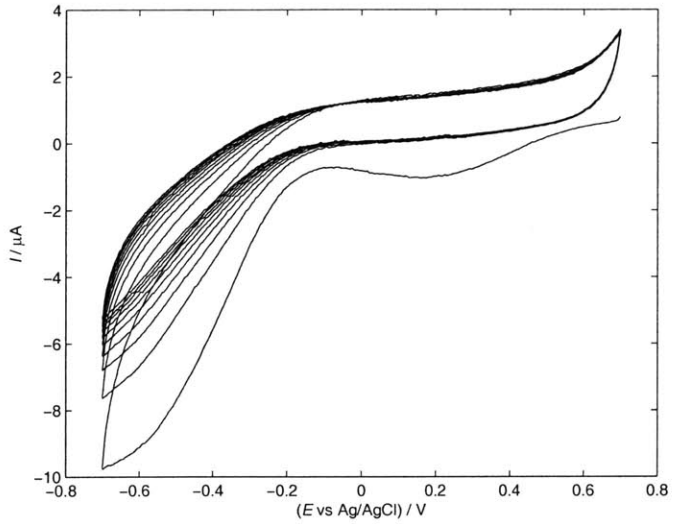

Figure 5-1: Adsorption scans of 1 mM peptide in solution, showing current (I) as a function of applied potential (E). Ten scans from +0.7 to –0.7 V were performed successively, at a scan rate of 100 mV/s. The strongest signal corresponds to the first scan.

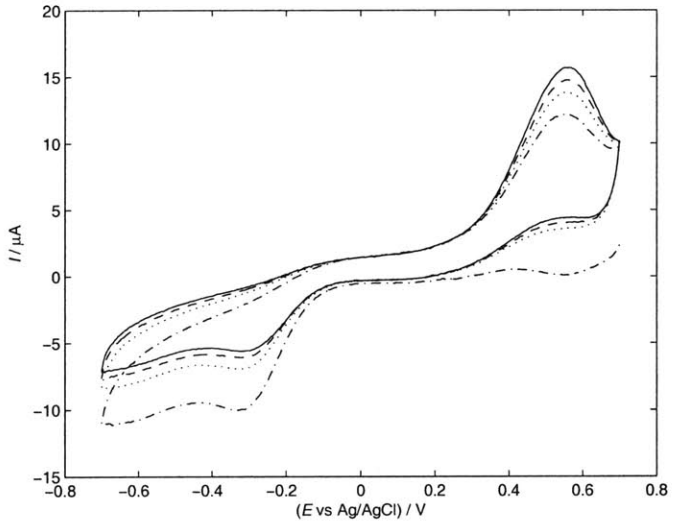

Figure 5-2: Cyclic voltammetry of 25 mM MOPS buffer. Ten scans were performed from +0.7 V to –0.7 V at 100 mV/s. For clarity, only scans 1 (dashed/dotted), 4 (dotted), 7 (dashed), and 10 (solid) are shown.

from reaching the surface.

The signals in Figure 5-1 may reflect only the peptide being adsorbed onto the surface during that particular scan, rather than all the peptide accumulated on the surface. In other words, while the total amount of peptide on the electrode surface is expected to increase with each scan, it increases by a smaller amount each time. (Mathematically, this can be described by a Langmuir adsorption model, which is based on the idea that there are a fixed number of surface sites available for adsorption [48].) In this case, the current would not be due to reversible oxidation and reduction, as seen for ferricyanide (Chapter 3), because then the peptide already adsorbed onto the surface should also contribute, and the signal should increase with successive scans. Also, as with MOPS, there are no obvious redox-active centers in the peptide.

However, it is possible that some sort of charge transfer accompanies the adsorption. When the peptide is adsorbed, a bond is formed between the gold of the electrode and the sulfur in the cysteine residue. The oxidation states of the sulfur and gold atoms might change with the formation of this bond; sulfur can occupy a range of oxidation states, and the electrode can easily give up or gain electrons as well. If the actual adsorption event involves the transfer of charge between the peptide and electrode, then the decreasing signal is reasonable. In this case, Figure 5-1 also indicates that as the applied potential is made more reducing, the rate of adsorption increases.

The total charge transferred over the 10 scans was calculated to check whether it corresponded to a monolayer of peptide. For each scan, the net charge (forward scan – reverse scan) was found by integrating the current numerically with respect to time. A background current was assumed to account for how the charge transferred approaches a non-zero value, and the signal from the final scan was defined as the background. Once this adjustment has been made, the total charge transferred during the peptide scans is 31 μC (Table 5.1).

Using equation 3.10, this corresponds to a surface coverage Γ of 4.6×10^{-9} mol/cm^2. To check if this is a reasonable result, the volume of the peptide was estimated [1]. For simplicity, the peptide was assumed to be a cube, and packed closely on the electrode surface. Furthermore, we assumed that $n = 1$ and that A equaled the geometric area. With these conditions, the theoretical surface coverage was calculated to be 2.0×10^{-10} mol/cm^2.

The experimental value of Γ is about 20 times greater than the theoretical value. Some of this discrepancy is due to roughness on the electrode surface, which makes the surface area larger than the geometric area. Also, the area occupied by a molecule of peptide is difficult to estimate, since the peptide only attaches through the cysteine S atoms. Thus, given the simplifying assumptions,

Scan	Charge (μC)	Charge – Background
1	35.5	17.6
2	22.7	4.8
3	20.9	3.0
4	20.0	2.1
5	19.4	1.5
6	18.9	1.0
7	18.7	0.8
8	18.4	0.4
9	18.0	0.1
10	17.9	0
Total	210.6	31.4

Table 5.1: Charge transferred during peptide loading scans, based on Figure 5-1. The final column was obtained by defining charge transferred during the last scan as background.

this may be a satisfactory result; it at least suggests that charge transfer due to adsorption is not a completely unreasonable model for the peptide signals.

5.1.2 Protein Signals

The protein signals were qualitatively similar to the peptide ones; the signal was strongest during the first scan, and decreased during subsequent scans (Figure 5-3, top). However, while the peptide signal was very consistent between experiments, the protein signal sometimes varied. Occasionally, the current during the first scan would be noticeably smaller, and in these cases, the decrease during subsequent scans was also less apparent (Figure 5-3, bottom).

When the total charge transferred over 10 scans was calculated, the result after correcting for background current was remarkably similar to total charge transferred during peptide loading (Table 5.2), especially considering that the scans were done over different applied potential ranges and at different scan rates. (For protein adsorption, the current is about an order of magnitude smaller than for peptide adsorption, but this effect is balanced by the slower scan rate, which causes each scan to take a longer time.) This may be simply a matter of coincidence, or it may support the idea of charge transfer associated with adsorption. The interaction between peptide and protein is most likely due to electrostatic forces [7], so it is not clear that any electron transfer would be associated with the adsorption of protein onto the peptide-modified surface.

The protein signals during adsorption are similar to those presented in [4], but there are some noticeable differences. The peak currents are smaller in this work, which is partly due to the fact

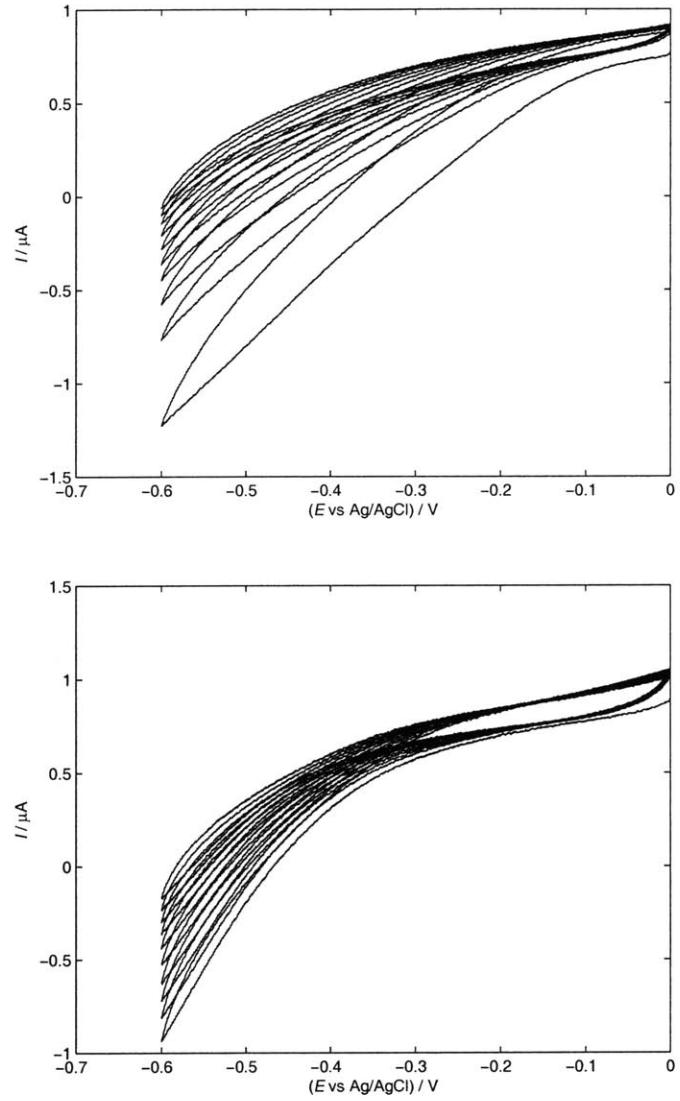

Figure 5-3: Adsorption scans of 35 μM MMOH in solution. Ten scans were performed from 0 to -0.6 V at 5 mV/s. Occasionally, the first signal was weaker and the subsequent decay was less obvious (bottom); the top figure is more representative.

Scan	Charge (μC)	Charge – Background
1	29.6	18.0
2	15.3	3.6
3	14.8	3.2
4	13.7	2.1
5	13.8	2.2
6	13.0	1.3
7	12.6	1.0
8	12.1	0.5
9	11.8	0.2
10	11.6	0
Total	147.1	30.9

Table 5.2: Charge transferred during protein loading scans, based on Figure 5-3 (top). As with peptide, charge transferred during the final scan was defined as background.

that a smaller gold electrode was used. However, the shape of the signal is also slightly different. In [4], the current remains close to zero during the first part of the forward scan, and then increases quickly once the applied potential is sufficiently negative. For later scans, not only is the peak current reduced, but the signal also becomes nonzero at less negative potentials. In this work, the protein signals are nonzero at the beginning of the scan, and the increase in current is more gradual and does not shift with successive scans.

These differences are difficult to interpret. They may be caused partly by differences in background current caused by the physical configurations of the two systems, but other reasons for the discrepancies are not known. In any case, it was assumed that adsorption of MMOH had occurred, and further experiments were carried out.

5.1.3 Scan Rate Dependence

For diffusion-controlled species such as ferricyanide, the peak current is proportional to the square root of the scan rate, as seen in Equation 3.6. For adsorbed species, however, the peak current is directly proportional to the scan rate [4]; these relationships provide a useful diagnostic of whether a particular species is surface-attached or freely diffusing in solution.

Cyclic voltammetry of MMOH was done at scan rates between 5 and 50 mV/s, before and after adsorption of protein. In both cases, the electrode surface had already been modified with peptide. Some adsorption most likely occurs during the "before" set of scans, but this is assumed to be minimal.

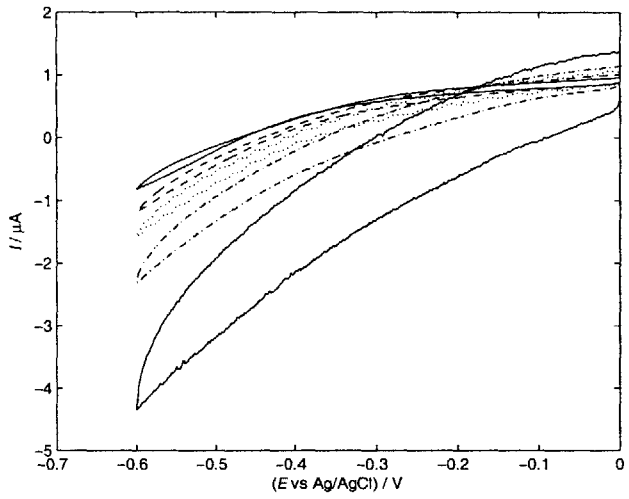

Figure 5-4: Cyclic voltammetry of 35 μM MMOH in solution, before adsorption. Scans were recorded at 50 (solid line, stronger signal), 20 (dashed/dotted line), 10 (dotted line), 5 (dashed line) and 2 (solid line) mV/s.

The scans taken before adsorption show that $i_p \sim v^{1/2}$, as expected (Figure 5-4). Again, there are qualitative differences between this work and [4]; most notably, here the current continues to increase in magnitude until the switching potential is reached, rather than reaching a maximum and then leveling off or decreasing slightly.

When the scans are repeated after adsorption, the results are very similar to those obtained beforehand (Figure 5-5). The peak current still appears to be proportional to $v^{1/2}$. As confirmation, (ln i_p) can be plotted against (ln v); the slope gives the value of k, where $i_p \sim v^k$. In this case, the plot yielded a slope of 0.50, with a correlation coefficient of unity. This strongly suggests that either the protein did not get adsorbed, or the signal is due to another species. In the latter case, the current might be expected to be lower after adsorption, since the presence of large enzyme molecules would block access to the electrode surface, but this effect is not seen.

It is possible that the effectiveness of protein adsorption varied from one experiment to the next, and perhaps this set of data corresponds to a particularly ineffective adsorption. For comparison, when a different set of peak currents after adsorption was plotted against $v^{1/2}$, the result was clearly non-linear, while a plot of i_p versus v appears to fit a straight line relatively well ($R^2 = 0.98$). These results are shown in Figure 5-6. However, a ln-ln plot yielded a slope of 0.58, still much closer to the diffusion-controlled limit than the adsorption one.

Another possibility is that the theoretical limit of $k = 1$ does not apply in this situation. This

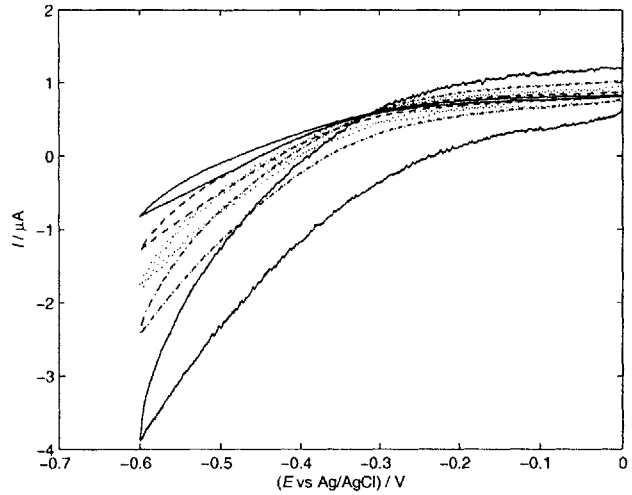

Figure 5-5: Cyclic voltammetry of 35 μM MMOH in solution, after adsorption. Scans were recorded at 50 (solid, stronger signal), 20 (dashed/dotted), 10 (dotted), 5 (dashed), and 2 (solid) mV/s.

limit describes the case of a redox-active species adsorbed directly to the electrode surface; in this case, mass transport is not limiting, since the molecules do not need to diffuse to the surface. Some methods of enzyme immobilization do appear to require transport to the surface; for example, when myoglobin (Mb) is contained within a thin film of surfactant, the signal is much stronger than that of Mb in solution, but still diffusion-controlled [8]. It is possible, though perhaps unlikely, that a similar effect could be seen for MMOH and the peptide layer. The role of the peptide appears to be partly to "cushion" MMOH so it does not denature at the electrode surface, implying that the peptide forms a impenetrable layer between enzyme and electrode. On the other hand, if this conceptual picture is correct, the distance between the electrode and the active site of the enzyme may be too large for effective electron transfer. Since the peptide bonds are free to rotate and the interaction between peptide and enzyme is electrostatic in nature, the peptide layer is flexible, and movement of the MMOH molecules relative to the electrode is also possible. This may explain why the post-adsorption data still appears diffusion-controlled, while the protein-modified electrode does respond to the concentration of substrate, as seen below.

5.2 Acetonitrile Experiments

Initial concentration studies were carried out using acetonitrile as the substrate, rather than methane. This was done for practical reasons; making solutions of a known concentration of

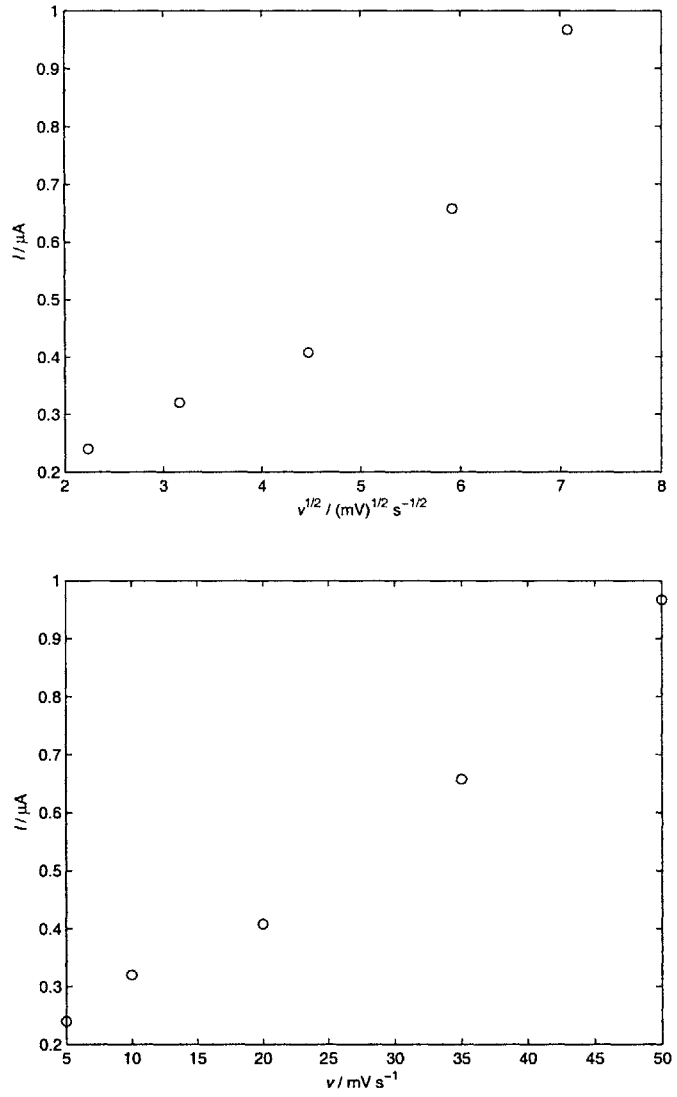

Figure 5-6: MMOH peak currents as a function of scan rate, after adsorption. These results were obtained on the analog system used in the early stages of this work (see Appendix).

dissolved gas is more difficult, and we wanted a simple check of whether increasing substrate concentration led to any sort of increased signal.

Acetonitrile is oxygenated by MMO in a reaction analagous to that of methane, producing glycolonitrile [51]:

$$CH_3CN + NADH + H^+ + O_2 \rightarrow HOCH_2CN + NAD^+ + H_2O \tag{5.1}$$

In the first experiment, four 5 μL aliquots of dilute acetonitrile solution were added successively to the MOPS buffer, giving CH_3CN concentrations up to about 175 μM. At this stage, the potentiostat was not yet computer-driven (see Appendix), and data was collected on a chart recorder; the results are shown in Figure 5-7. A plot of peak current against concentration shows a clear increase in signal with increased [CH_3CN] (Figure 5-8). Between 5 to 15 μL of added acetonitrile solution, the signal increases linearly ($R > 0.999$). When the final aliquot was added, the signal remained the same; this could be due to experimental error, such as poor microsyringe technique, but it is more likely that the signal reaches a maximum at some concentration and then cannot increase further. This is qualitatively consistent with the Michaelis-Menten model of enzyme kinetics, in which there is a maximum rate of enzyme turnover, and increasing the substrate concentration past the saturation value has no further effect on reaction rate [27]. However, the signal at zero concentration is lower than what would be expected from extrapolating the results from 45–130 μM.

In this experiment, the MOPS solution had been degassed with a slow stream of argon for 3 minutes before the first addition of acetonitrile. After the final aliquot was added, the solution was degassed for an additional minute, and then a scan was recorded; this process was done twice. As shown in Figure 5-7, the signal clearly decreases as argon displaces the dissolved oxygen in solution. This suggests that the signal most likely does come from MMOH adsorbed onto the electrode surface, since the response depends on both substrate and oxygen (Equation 5.1).

After the computer-driven system had been set up, this experiment was carried out once more. The MOPS buffer was degassed with argon as before, and this time, five 3 μL aliquots of diluted acetonitrile were added, giving a final concentration of about 130 μM. The results are shown in Figure 5-9; the peak currents increase with concentration, but in a nonlinear manner. However, one result of digital data acquisition is that the total charge transferred can be found as well (see Appendix). Both the amount of charge transferred on the forward scan and the net charge trans-

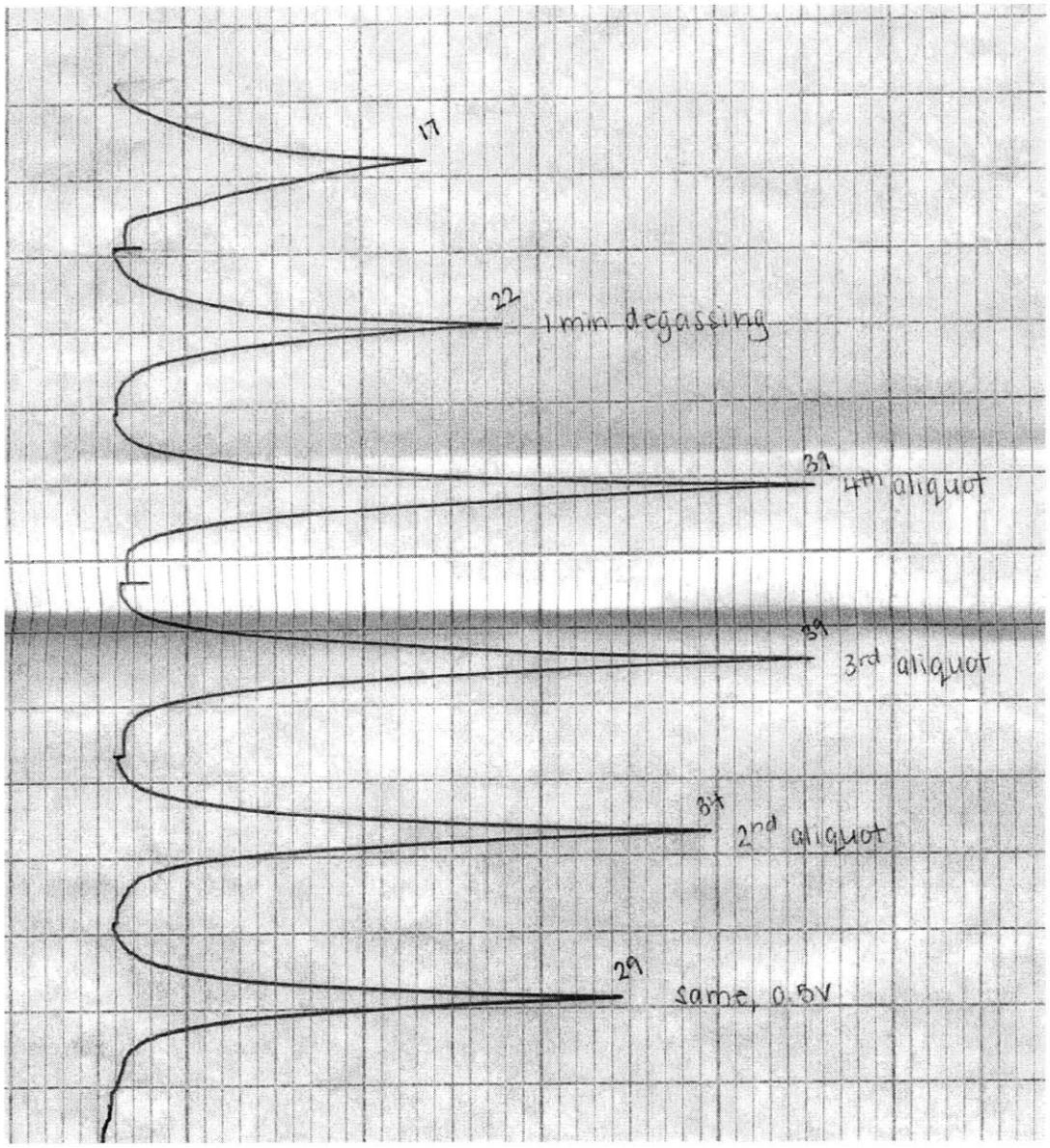

Figure 5-7: Chart recorder results showing current at various acetonitrile and oxygen concentrations (see text). Scans were performed from 0 to –0.6 V at 50 mV/s. Each small marking in the horizontal direction represents 5 mV voltage, which corresponds to 0.05 μA current (see circuit diagram, Figure A-1). Instead of the typical cyclic voltammogram, which shows current as a function of applied potential, here current is displayed as a function of time, which increases in the vertical direction.

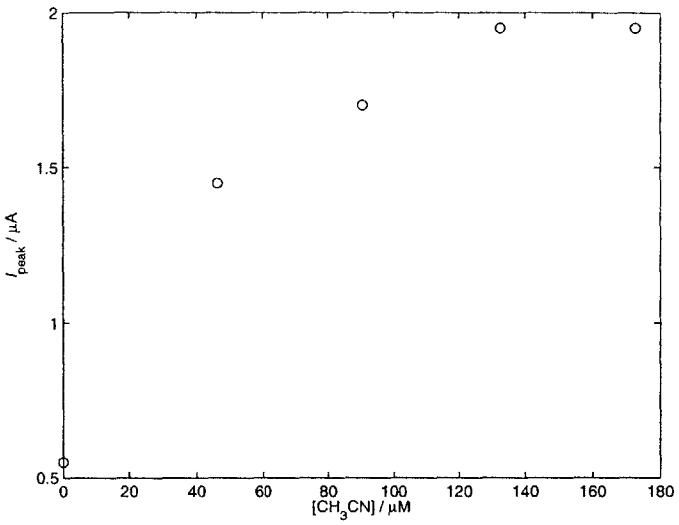

Figure 5-8: Peak current as a function of acetonitrile concentration

ferred (forward – reverse) are concentration-dependent, and for $[CH_3CN] < 80$ μM, the relationship is linear ($R > 0.99$). Unlike in the previous experiment, this time the data point corresponding to zero concentration falls on the line.

Again, these results are qualitatively consistent with a Michaelis-Menten kinetics model, where there is a limiting rate of enzyme turnover. In the model, however, reaction rate is directly proportional to concentration at low values of C and constant at high values, with a transitional region in between. Here, the electrical signal is directly proportional up to a certain concentration, and then there is actually a slight decline. However, the decreased signal may not be statistically significant – the acetonitrile experiments were not repeated, so this is only a guess – or it may reflect a slight decrease in oxygen level. In any case, this set of results strongly supports our original hypothesis of an analytical relationship between signal and substrate concentration. If the concentration of acetonitrile increases, we expect MMOH to turn over faster (assuming the concentration is in the $v \sim C$ region of the Michaelis-Menten model). From Equation 5.1, we see that this corresponds to more electrons being passed to MMOH in the same amount of time, and thus to an increase in charge transferred.

The acetonitrile experiment was then repeated without the initial three-minute degassing, to see what the effect of increased oxygen concentrations would be. The results showed two different types of signal shapes (Figure 5-10). At low concentrations, the current during the forward scan increased steadily over the entire scan. At higher concentrations, the current increased sharply

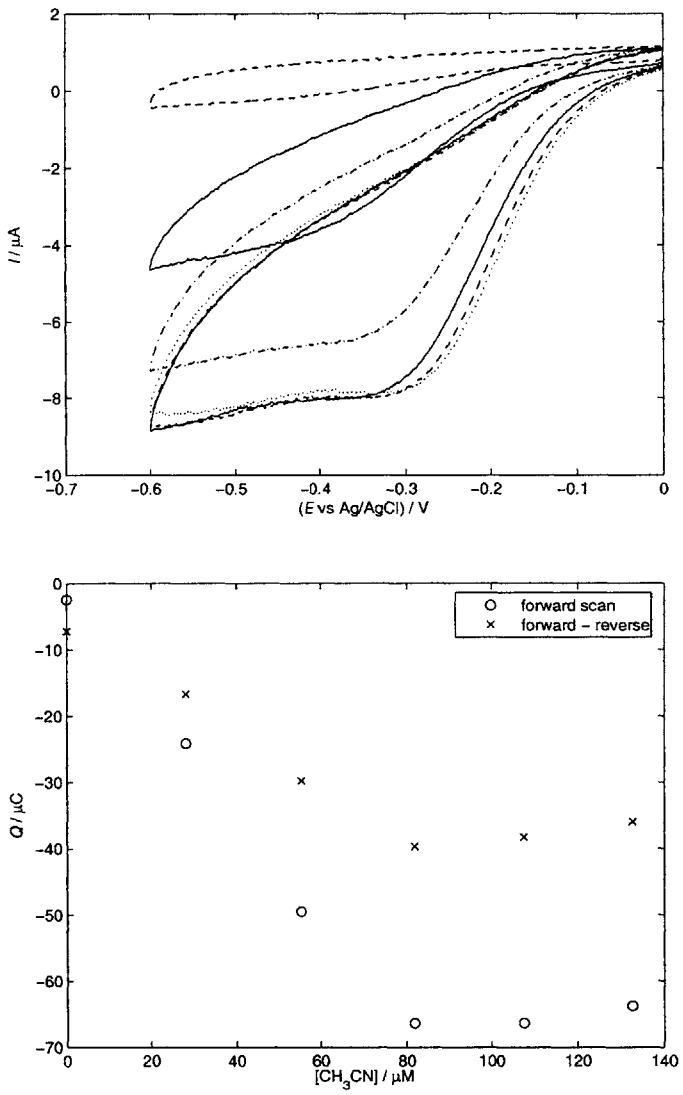

Figure 5-9: Top: Acetonitrile concentration series, $v = 50$ mV/s, degassed. Scans were taken at 0 (dashed, weakest signal), 28 (solid), 55 (dashed/dotted), 81 (dotted), 108 (dashed), and 133 (solid) μM [CH_3CN]. Bottom: Charge transferred as a function of acetonitrile concentration.

around 0.2–0.3 V, and then remained at this level for the rest of the scan, without responding to further changes in applied potential. For comparison, when the solution had been degassed, the signal was similar to the high-concentration case; at low concentrations, the increase in current was more gradual, but still generally reached a plateau.

When the solution is not degassed, it can be assumed that oxygen is close to saturation, that is, around 9 mg/L or 300 μM. When $[CH_3CN] > 80$ μM, the signal changes as described above, and the total charge transferred is much greater. We suggest that this type of signal indicates that catalytic turnover is happening; at a certain applied potential, electron transfer to MMOH becomes favorable, and the enzyme begins to convert acetonitrile to glycolonitrile. Since the reaction with substrate is catalytic, the flow of current becomes much greater. Also, once the applied potential is sufficiently negative to allow electron transfer to MMOH, a further reduction in potential will not have an additional effect.

The question remains of why this does not happen at low substrate concentrations when oxygen level is high. The catalytic cycle of MMO (Figure 2-2) shows that the active site binds oxygen first, and goes through several intermediates before binding and reacting with methane. One possibility is that the negative applied potential and presence of oxygen allows the formation of the Q intermediate, and then there is not enough substrate to react with all of the enzyme molecules. Then, only a fraction of enzyme molecules would return to the H_{ox} state and be ready to react with another molecule of substrate; the others might effectively be stuck partway through the cycle. On the other hand, if oxygen and substrate levels are both low, then only some of the enzyme molecules are able to catalyze the reaction. But in this case, the other molecules of MMOH are still in the H_{red} state (after the applied potential is negative enough to reduce H_{ox}), and so substrate molecules approaching the surface experience a larger effective amount of enzyme.

Finally, to check whether the concentration-dependent signal was in fact due to catalytic MMOH activity, a control experiment was performed in which no protein was adsorbed onto the electrode surface. The clean electrode was coated with peptide, as before, and then scans were taken at the various acetonitrile concentrations. As expected, there was no concentration dependence (Figure 5-11). However, the signal seen in the no-protein case is similar to the signal that the protein-containing system approaches at high concentration, regardless of oxygen level. In fact, when the 130 μM scans are compared, all three voltammograms are virtually identical.

To provide a comparison, the control experiment (electrode modified with peptide only) was repeated with a solution of MOPS only, without acetonitrile. Scans were taken at scan rates between

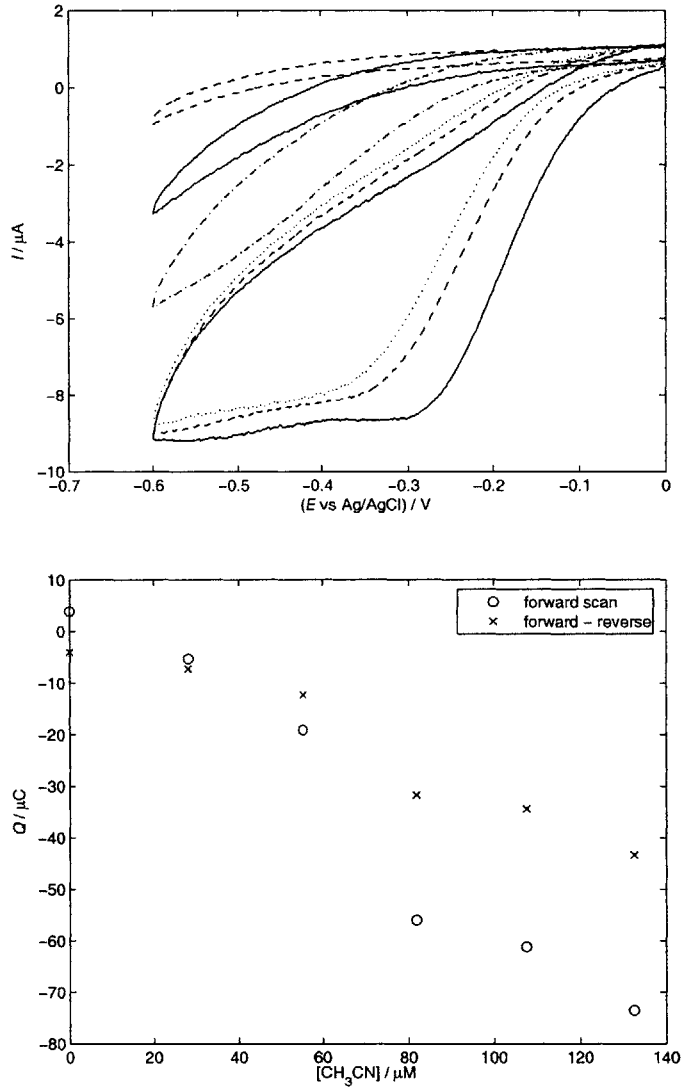

Figure 5-10: Top: Acetonitrile concentration series, $v = 50$ mV/s, air-saturated. Scans were taken at 0 (dashed, weakest signal)), 28 (solid), 55 (dashed/dotted), 81 (dotted), 108 (dashed), and 133 (solid, strongest signal) μM [CH_3CN]. Bottom: Charge transferred as a function of acetonitrile concentration.

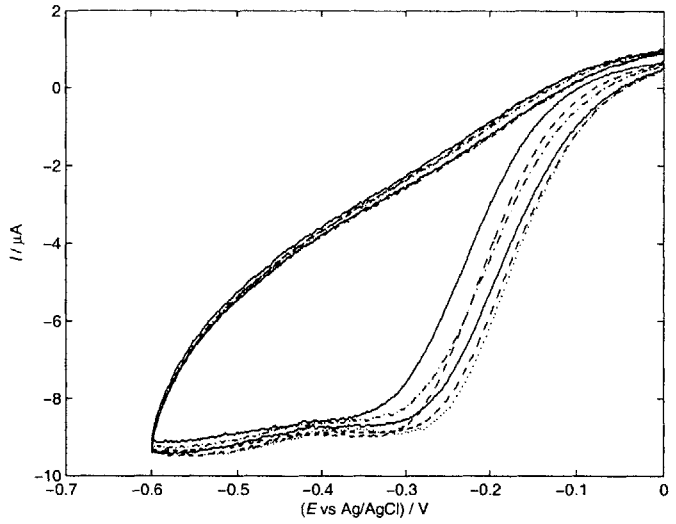

Figure 5-11: Acetonitrile control experiment without adsorbed MMOH. Scans were taken at the same concentrations as in Figures 5-9 and 5-10, at 50 mV/s.

5–50 mV/s, and with the exception of the 50 mV/s case, the signals are qualitatively similar those in the acetonitrile control experiment (Figure 5-12). The signals exhibit what was described earlier as a "catalytic" shape, so an alternative explanation for the acetonitrile results may be necessary.

Conceptually, a picture involving resistances of the peptide and protein layers may be useful. A similar model applies to mass transfer across an air-water interface; under certain conditions, diffusion across either air or water may be neglected because the other is clearly limiting, but at other times, both layers contribute to the mass transfer rate (in other words, the "resistance" of both the air and water layer must be considered). In this case, it appears that at high acetonitrile concentration, the resistance of the MMOH layer approaches zero, so that electron transfer is only limited by the peptide layer. However, a molecular-level explanation of the signal shape is not clear at this time.

5.3 Methane Experiments

Since the acetonitrile results were promising, similar experiments were then carried out using methane as the substrate. Because methane is a gas, preparing solutions of known concentration was more difficult than in the case of acetonitrile. To prepare these solutions, two approaches were considered.

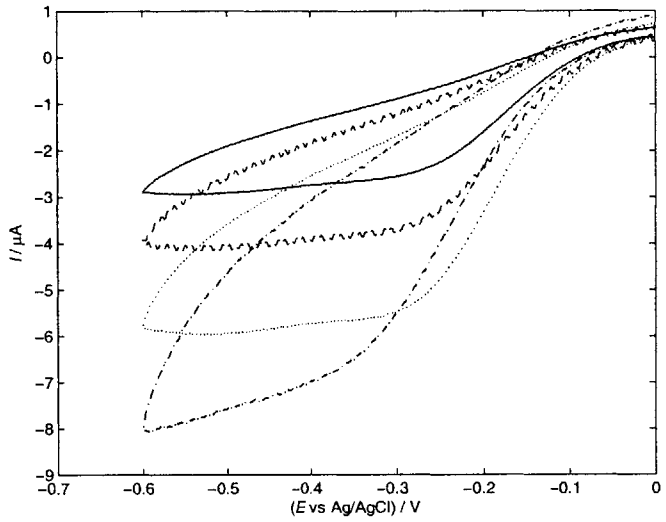

Figure 5-12: Cyclic voltammetry of 25 mM MOPS solution at peptide-modified electrode. Scans were taken at 5 (solid), 10 (dashed), 20 (dotted), and 50 (dashed/dotted) mV/s.

mL CH_4	mL O_2	$[CH_4]$, μM	$[O_2]$, mg/L
1	2	75	5.0
2	0	150	0
3	2	225	5.0

Table 5.3: Concentrations of methane and oxygen, using the headspace equilibration method and assuming $T = 298$K. In all cases, the total volume of gas was made up to 20 mL using helium; 5 mL of MOPS solution was used.

One approach is that of headspace equilibration, in which known amounts of gas and liquid are contained in a closed system. In this case, 30-mL wetted glass syringes were filled with 20 mL of a gas mixture made up of methane, oxygen and helium. 5 mL of MOPS buffer was added to each syringe, and equilibration was achieved by placing the syringes on a motorized shaking apparatus for 30 minutes. The final concentration of methane in solution depends on the partial pressure of methane in the original gas mixture, the volumes of gas and water, and the dimensional Henry's constant:

$$C_w = \frac{P_g V_g}{V_w RT + V_g H} \tag{5.2}$$

Examples of suitable mixtures are given in Table 5.3.

mL CH_4	$[CH_4]$, μM
2	150
4	300
6	450
8	600

Table 5.4: Methane concentrations for bubbling experiments. As in Table 5.3, 0 or 2 mL of O_2 was used for oxygen concentrations of 0 or 5 mg/L; volume of gas totaled 20 mL. $[CH_4]$ values are rounded slightly.

An alternative method involves making up the same gas mixtures inside the syringe, and then bubbling them directly through 0.2 mL of MOPS solution in the small-volume cell. If equilibration between the gas phase and liquid phase is assumed to be fast relative to the total amount of time over which bubbling occurs, then the concentration in solution approaches the saturation value:

$$(C_{sat} - C_w) = C_{sat} e^{-H(V_g/V_w)} \tag{5.3}$$

where C_w is the concentration in solution, C_{sat} is the saturation value (for gas mixtures, the concentration of solution in equilibrium with an infinite volume of gas phase), H is the dimensionless Henry's constant, and V_g and V_w are the volumes of gas and water. This approach seemed preferable, since the need for a 30-minute shaking period was eliminated, excess MOPS solution was not used, and it was easier to blanket the solution with a small volume of gas mixture. As it turns out, the assumption of fast equilibration is a significant one, and the bubbling approach may not have been the best choice.

The methane concentrations in Table 5.4 were used in most experiments.

5.3.1 Preliminary Experiments

The acetonitrile results showed that electrical signal, specifically total charge transferred, was dependent on both substrate and oxygen concentration. As a first step, we investigated whether this was also the case when methane was used as the substrate.

The results are shown in Figure 5-13. The signal strength increased with methane concentration, and the presence of oxygen at 5 mg/L caused both signals to be significantly enhanced. Again, this strongly suggests that the signal is due to MMOH on the electrode surface. Since both oxygen and methane are needed for the catalytic cycle to proceed, the dramatic effect upon increasing $[O_2]$ is not surprising. Also, when oxygen was present, increasing methane concentration resulted

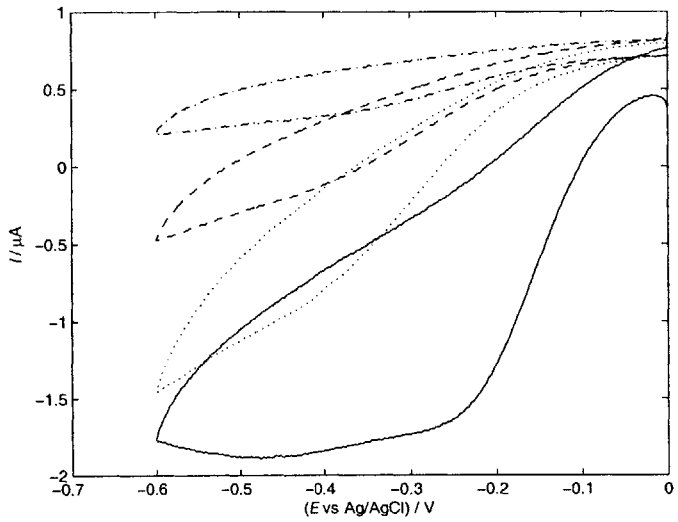

Figure 5-13: Effects of methane and oxygen concentrations, scans taken at 50 mV/s. Concentrations: 150 μM [CH_4], no oxygen, dashed/dotted line; 300 μM [CH_4], no oxygen, dashed line; 150 μM [CH_4], 5 mg/L [O_2], dotted line; 300 μM [CH_4], 5 mg/L [O_2], solid line. For clarity, the Matlab `smooth` function was applied an additional time to all methane data sets.

in a change in signal shape. As discussed previously, this may correspond to catalytic turnover of MMOH occuring when both oxygen and substrate concentrations are reasonably high.

Next, the effect of oxygen concentration was investigated separately. Figure 5-14 shows a clear and consistent dependence on [O_2]; the signal increased with dissolved oxygen concentration, and the 20% oxygen case (which corresponds to 10 mg/L) was very similar to the air-saturated case. This could mean that oxygen is being directly reduced at the electrode surface. An experiment in which the electrode was modified with peptide only, and then [O_2] was varied, may be useful to eliminate or confirm this possibility. Another possibility is that the presence of oxygen is causing MMOH turnover to increase, which seems less likely, since no methane is present.

A control experiment was again performed, with peptide but no protein adsorbed onto the electrode. In this case, as with acetonitrile, the signal did not change as substrate concentration increased (Figure 5-15).

5.3.2 Scan Rate Effects

We also wished to explore the effect of changing the scan rate. A slower scan rate means that a voltammogram over a given potential range takes a longer time, so that the diffusion layer over

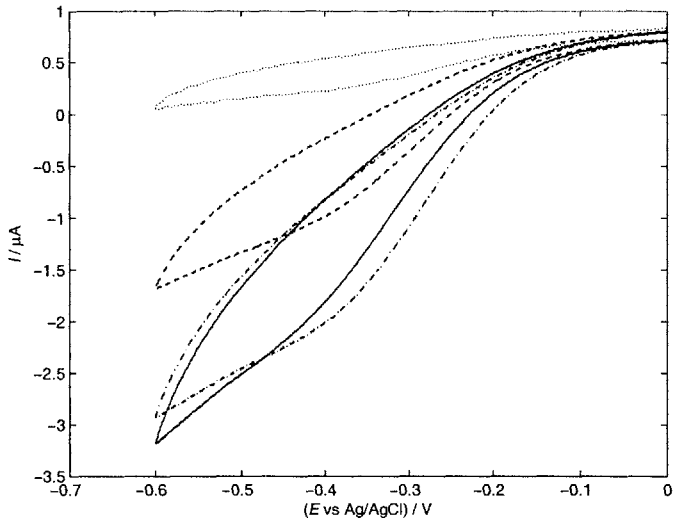

Figure 5-14: Effect of oxygen on MMOH electrochemistry; scans taken at 50 mV/s. Conditions: no bubbling (saturated), dashed/dotted; helium only, dotted; 5 mg/L [O_2], dashed; 10 mg/L [O_2], solid line.

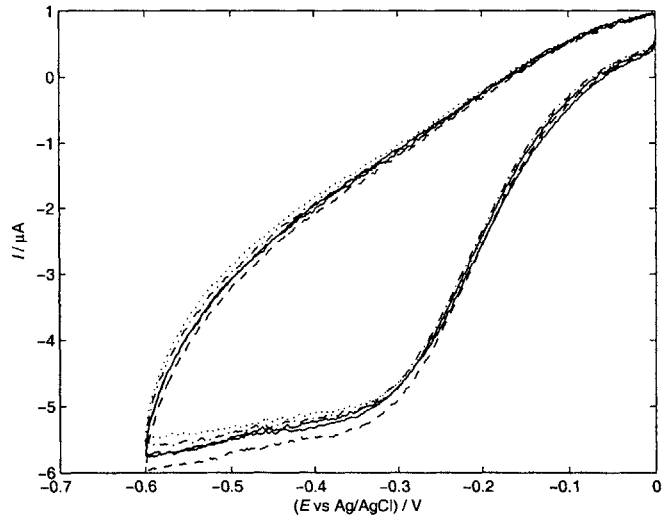

Figure 5-15: Methane control experiment without adsorbed MMOH. Scans were taken at 0, 150, 300, 450, and 600 μM [CH_4]. Signals are stronger than those in Figures 5-13 and 5-14, but similar to others reported later in this section.

which concentration is depleted (δ_c in Figure 3-3) extends farther from the electrode surface. As a result, flux to the electrode surface is reduced, and peak currents are smaller [43]. In this case, we were interested in whether the plateau region of the catalytic signal might be due to transport effects or to the intrinsic turnover rate of the enzyme. If the plateau level of current does not depend on scan rate, for a given concentration of oxygen and methane, that might indicate that the maximum turnover rate of MMOH is the limiting factor. If, on the other hand, the current decreases with scan rate, then the signal would be at least partially diffusion-limited.

In the first experiment, the effects of increasing [CH_4] were studied at scan rates of 50 and 20 mV/s. The 50 mV/s scans were conducted first, and concentration was increased to 900 μM before the broader, possibly catalytic signal shape was seen (Figure 5-16). From this data, it appears that signals exhibiting a more concave shape can also show a linear relationship between signal strength and concentration (R = 0.98 for the forward scan); the low-concentration scans in Figure 5-10 illustrate this point as well. The charge transferred during the forward scan often appears to show a more consistent relationship, so further discussion will focus on this value, rather than the net charge transferred.

The concentration series was then repeated at a scan rate of 20 mV/s, starting with low methane concentration. Surprisingly, the results showed essentially no concentration dependence; in fact, even the blank exhibited a pronounced, broad signal. There appears to be some sort of hysteresis effect, where the order in which scans are taken affects the results. These results (Figure 5-17) suggest that the enzyme might have retained some of the previously available methane, especially considering the high concentrations reached in the 50 mV/s scans.

In terms of microbiology, this makes some sense; methanotrophs use methane as their source of both carbon and energy, and it would be advantageous if methane available at one time could be stored for later use once oxygen was available. On a molecular level, this would mean that the enzyme can bind methane away from the active site, and then transfer it to the active site once a suitable intermediate has been formed. Since there are significant hydrophobic sections of MMOH that play a role in binding methane and allowing access to the active site [46], it is at least possible that these two steps could happen at different times. This possibility is also supported by the kinetic studies done in [21], which are consistent with a mechanism in which an enzyme-substrate complex is formed first with methane, and then with oxygen.

To test whether hysteresis was occurring, the scan rate experiment was then repeated with a modified procedure. Instead of recording all the 50 mV/s scans first, followed by all the 20 mV/s

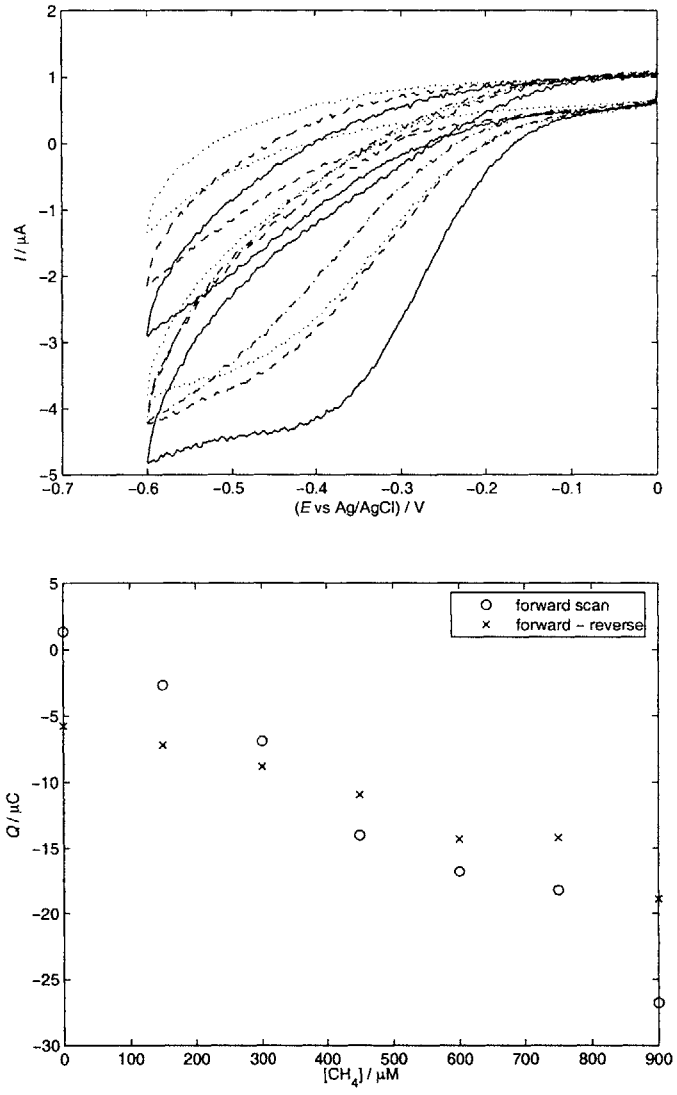

Figure 5-16: Methane concentration series, $v = 50$ mV/s, 5 mg/L $[O_2]$. Top: Scans were recorded at 0 (dotted), 150 (dashed), 300 (solid), 450 (dashed/dotted), 600 (dotted), 750 (dashed), and 900 (solid) μM $[CH_4]$. Bottom: Charge transferred as a function of methane concentration.

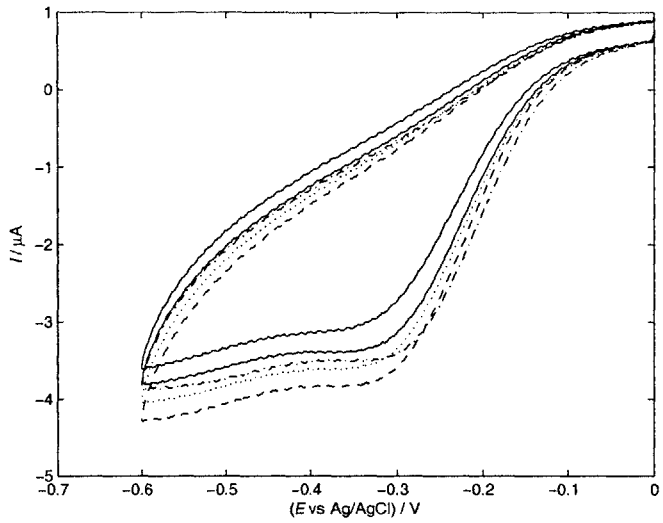

Figure 5-17: Methane concentration series, v = 20 mV/s, 5 mg/L $[O_2]$. Scans were recorded at 0 (solid, weaker signal), 150 (dashed/dotted), 300 (dotted), 450 (dashed), and 600 (solid) μM $[CH_4]$.

scans, both scans were taken at each methane concentration, starting with the blank. This time, the results at each scan rate were qualitatively similar (Figure 5-18). (The syringe used for the 450 μM trial was later found to be leaky, probably allowing air to enter, so those results should be neglected.) The peak (plateau) current is larger in the 50 mV/s scans, consistent with a diffusion-limited situation. However, this does not imply that catalytic turnover is not happening at all; rather, the rate at which new molecules of methane are supplied to MMOH is lower for the 20 mV/s scans, and so the rate of reaction is limited by transport.

Finally, this set of data shows that results are not necessarily consistent from one experiment to the next; in this case, increasing the methane concentration beyond 300 μM does not lead to further increases in signal strength. This may be due to the fact that a new layer of peptide and protein is adsorbed onto the electrode surface with each experiment, and will be discussed further in Chapter 6.

5.3.3 Effects of Oxygen

While the preliminary experiments showed a clear dependence on oxygen concentration, further investigation was desired. First, scans were taken over the usual concentration range (0–600 μM) with no oxygen present. With the exception of the 150 μM data point, the relationship between charge and concentration was quite linear (Figure 5-19); the signals were also much smaller than

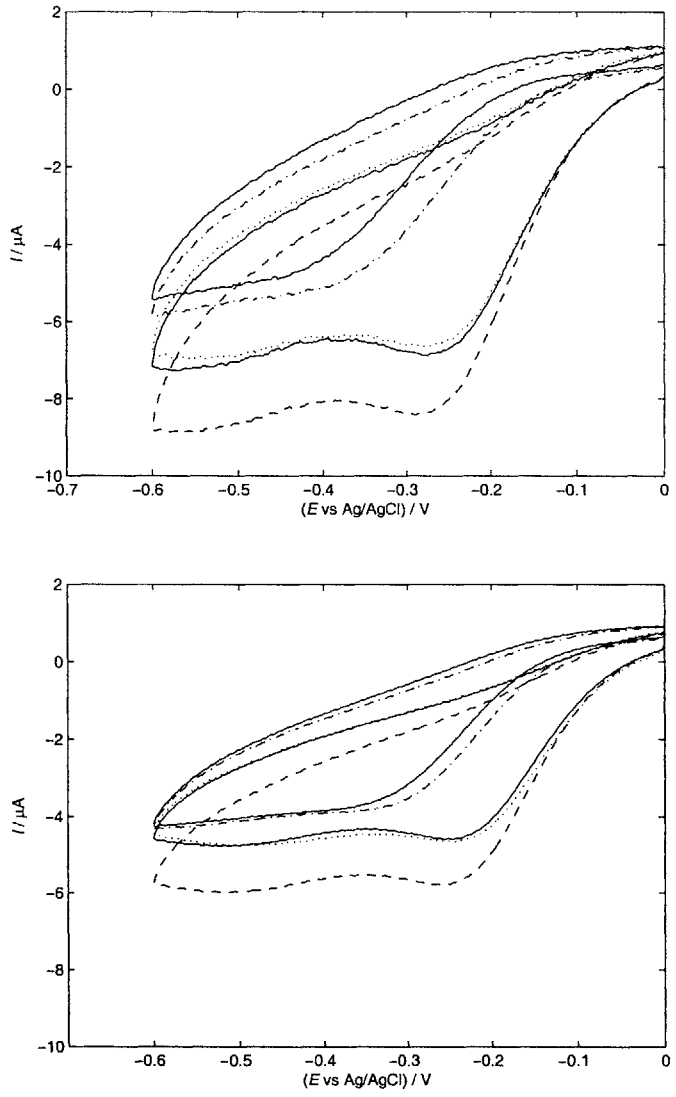

Figure 5-18: Scan rate and methane concentration dependence, 5 mg/L $[O_2]$. Scans were recorded at 0 (solid, weaker signal), 150 (dashed/dotted), 300 (dotted), 450 (dashed), and 600 (solid) μM $[CH_4]$, in the order described in the text. Top, 50 mV/s; bottom, 20 mV/s.

when oxygen was present.

Next, the concentration series was repeated with 5 mg/L of oxygen. Again, as in the scan rate experiment, the methane blank exhibited a strong, catalytic-type signal. It was suspected that a similar hysteresis effect was occurring due to storage of methane, so several consecutive scans were taken using the same solution. These results support the idea that excess methane has been stored by the enzyme, as the signal decreases before approaching a constant level (Figure 5-20). Presumably, the stored methane was consumed during the first two cycles, and the signal shown for scans 3–5 actually reflects the externally imposed oxygen and methane concentrations.

However, when the first 150 μM [CH_4] scan was then taken, the signal was again strongly catalytic, which was inconsistent with previous results of scans at this concentration. In fact, regardless of which scan number is considered for each methane concentration, the signals show no obvious methane dependence (Figure 5-21). The reasons for this are not clear, and it was simplest to assume that some storage effect, more complicated than what is described here, was affecting the results.

The experiment was then repeated; as with scan rate, methane was increased from lowest to highest concentration, and both oxygen concentrations were tested consecutively (Figure 5-22). This time, the signals for the oxygen-depleted cases were much stronger than in the previous experiment; it is difficult to tell if there is a significant inconsistency, or if the stronger signals are a result of alternating the 0 and 5 mg/L [O_2] trials. In this experiment, the signals are about twice as strong when oxygen is present, as seen in Figure 5-23. Both series exhibit a clear, monotonic concentration dependence for the forward scan data, though neither is quite linear. In the 5 mg/L [O_2] series, there appears to be random scatter, which may be due to the slow kinetics of methane equilibration between gas and liquid phase (discussed further in Chapter 6). In the oxygen-depleted series, the signal increases more than a linear relationship would indicate; the relationship actually appears to be more exponential. This result suggests that oxygen may be stored by MMOH as well, perhaps in the same hydrophobic regions that are capable of storing methane.

The methane experiments are summarized in Table 5.5. In Table 5.6, the best-fit lines relating charge transferred during the forward scan to concentration are compared for each of the 5 mg/L [O_2], $v = 50$ mV/s series. These show that while the signal clearly depends on [CH_4] within each experiment (except experiment 5, in which little dependence was seen as described previously), the results are not necessarily consistent between experiments. The intercept should be close to zero, and this is the case for two of the three best-fit lines. Even between those two lines, there is a

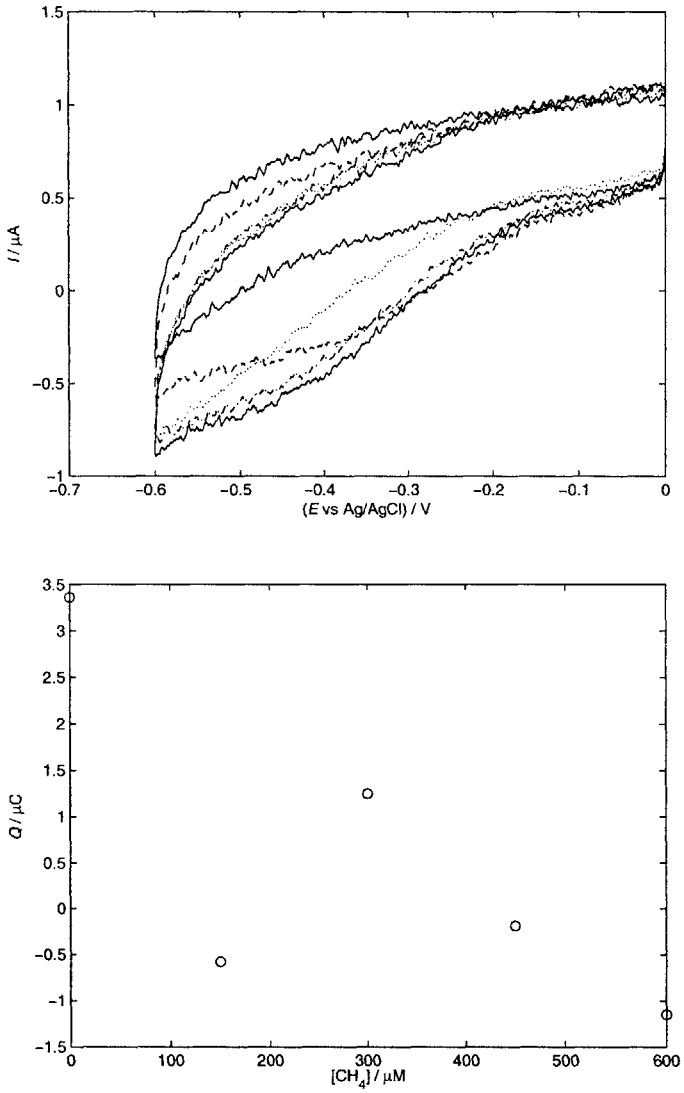

Figure 5-19: Methane concentration series, $v = 50$ mV/s, no oxygen. Top: Scans were recorded at 0 (solid, weaker signal), 150 (dashed/dotted), 300 (dotted), 450 (dashed), and 600 (solid) μM $[CH_4]$. Note scale of y-axis; noise is visible because signals are relatively weak. Bottom: Charge transferred during forward scan as a function of methane concentration.

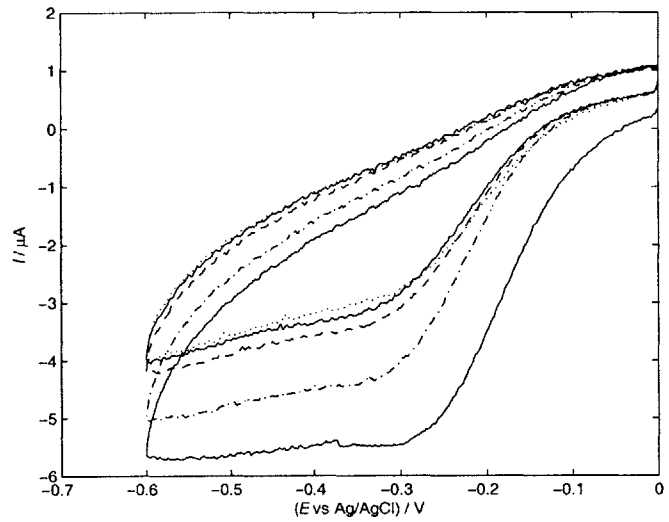

Figure 5-20: Effect of previously applied methane. Scans were done with 5 mg/L [O_2] and no methane after previous scans had been taken with up to 600 μM [CH_4]. Key: scan 1, solid (stronger signal); scan 2, dashed/dotted; scan 3, dotted; scan 4, dashed; scan 5, solid.

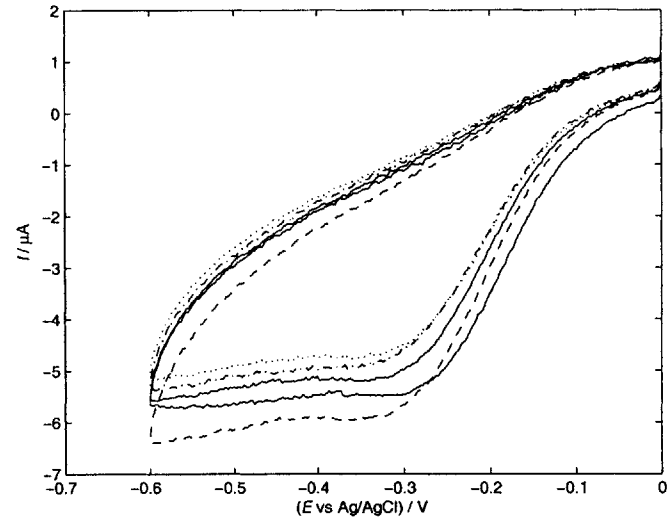

Figure 5-21: Lack of concentration dependence after previous exposure to methane. 50 mV/s scans were performed at 0 (solid, stronger signal), 150 (dashed/dotted), 300 (dotted), 450 (dashed), and 600 (solid) μM [CH_4]. The first scan at each concentration is shown here; qualitatively similar results were seen in subsequent scans.

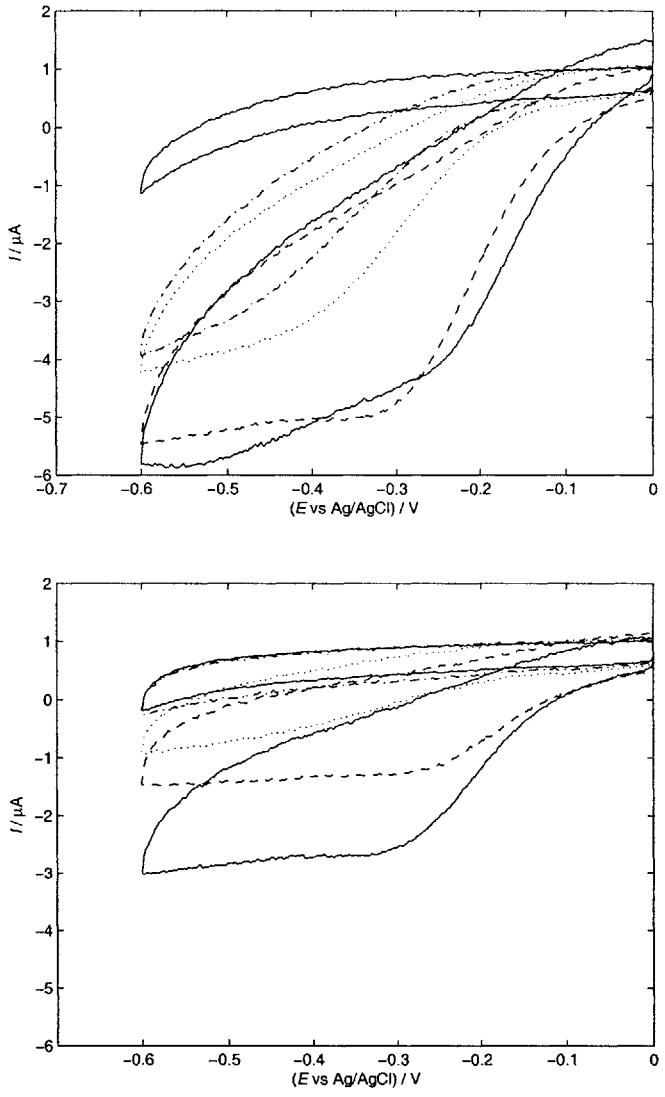

Figure 5-22: Oxygen and methane concentration dependence, $v = 50$ mV/s. Scans were recorded at 0 (solid, weaker signal), 150 (dashed/dotted), 300 (dotted), 450 (dashed), and 600 (solid) μM $[CH_4]$, in the order described in the text. Top, 5 mg/L $[O_2]$; bottom, no oxygen.

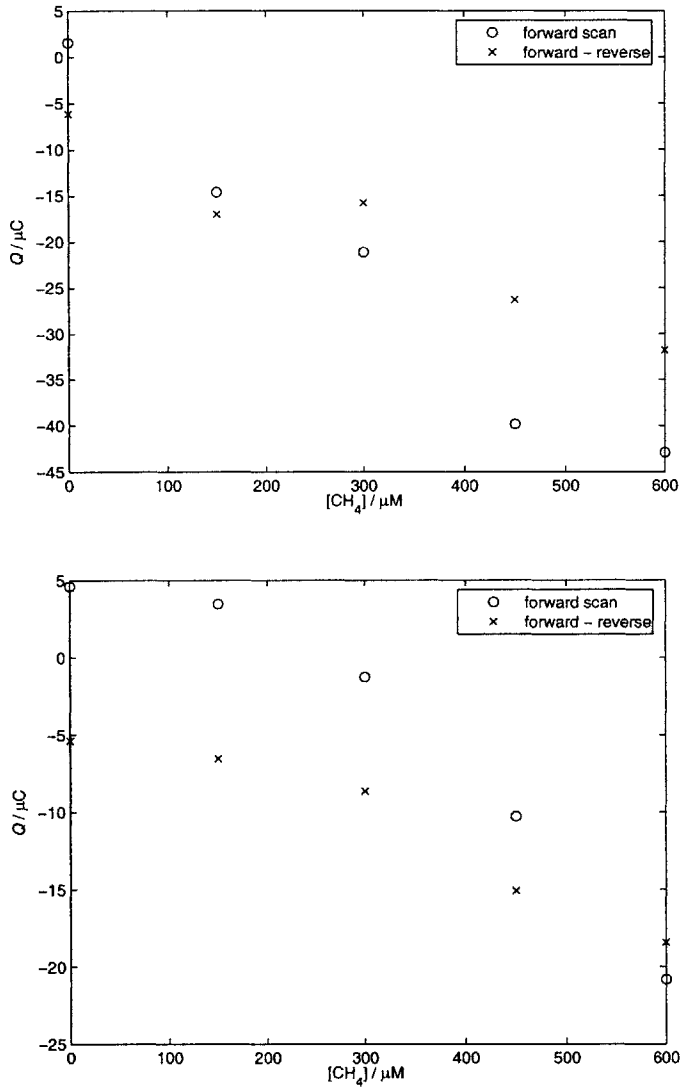

Figure 5-23: Charge transferred as a function of methane concentration. Top, 5 mg/L [O_2]; bottom, no oxygen.

Experiment	Description	Result
1	Preliminary	Oxygen and methane both affect signal strength; signals are relatively weak
2	Control (no MMOH)	Signal does not depend on $[CH_4]$
3	Scan rate, 50 mV/s and 20 mV/s done separately	50 mV/s series is close to linear through 900 μM; 20 mV/s series does not depend on $[CH_4]$, suggesting methane storage
4	Scan rate, alternating	Series have similar results, with stronger peak currents for 50 mV/s
5	Oxygen, 0 and 5 mg/L done separately	Oxygen-depleted signals are very small; 5 mg/L signals do not depend on $[CH_4]$
6	Oxygen, alternating	5 mg/L signals are twice as strong; oxygen-depleted series suggests possible O_2 storage

Table 5.5: Summary of experimental results for methane

Experiment	Best-Fit Line	R^2	Concentration Range (μM)
3	$y = -0.030x - 1.42$	0.976	$0 - 900$
4	$y = -0.062x - 17.3$	0.867	$0 - 300$
6	$y = -0.076x - 0.56$	0.961	$0 - 600$

Table 5.6: Best-fit lines for methane experiments in which $[O_2] = 5$ mg/L and $v = 50$ mV/s, relating charge transferred during forward scan to methane concentration. The relevant results from experiment 5 were omitted because essentially no $[CH_4]$ dependence was seen.

more than twofold difference in the slope. Judging from these results alone, the use of a MMOH-modified electrode for analytical measurements does not currently seem promising. However, we believe that a significant amount of the inconsistency may be due to experimental conditions that can be corrected; this topic will be further discussed in the following chapter.

Chapter 6

Discussion

6.1 Experimental Considerations

In terms of whether a MMOH-modified electrode can be used as an analytical sensor for methane, the results in Chapter 5 are somewhat unclear. At times, as with the degassed acetonitrile experiment, charge transferred was clearly dependent on substrate concentration. In the methane experiments, though, there was some experimental scatter and inconsistency, both within a particular experiment and between one experiment and the next.

There appear to be two main reasons for the scatter in the methane data. The first is related to the kinetics of methane partitioning between gas and liquid phase. As described in Chapter 5, bubbling causes the solution concentration of methane to approach the saturation level for a particular gas mixture, and is only dependent on the ratio of gas volume to solution volume (Equation 5.3). However, this result depends on the assumption of fast equilibration between gas and liquid. If this assumption does not hold, then the time over which gas is bubbled into solution must also be considered.

After the methane experiments had been completed, a qualitative check of partitioning kinetics was carried out. 5 mL of MOPS buffer was added to the electrochemical cell, and 50 mL of helium was slowly bubbled through the solution. Since $H \gg 1$ for oxygen (and methane), and $V_g/V_w = 10$, Equation 5.3 predicts that the oxygen concentration after bubbling should be essentially zero. However, when measured with an oxygen electrode, $[O_2] \simeq 5$ mg/L, indicating that the partitioning is kinetically limited.

The small-volume cell could not be used directly for this experiment, since it would have required an oxygen microelectrode. In the actual methane experiments, the bubbling time was about the

same, while $V_g/V_w = 100$. This test was designed to provide a general idea of whether kinetic limitation might have to be considered, and indicates that the solutions in the small-volume cell probably did not actually have the methane concentrations indicated in Table 5.4.

If this had been considered earlier, one possibility would be to still use the bubbling approach, but ensure that the bubbling was over the same time interval for each trial. However, a better approach is probably to use the method of headspace equilibration, described in Chapter 5. With acetonitrile, where there is no difficulty in making solutions of correct concentration, one set of results was almost perfectly linear (within concentration limits); we imagine that this result could be duplicated with methane, if more care were taken to prepare the solutions.

Another cause of experimental scatter stems from the fact that a new layer of peptide and protein was prepared for each experiment, and there is likely to be some difference in the adsorbed layer from one day to the next. It is not clear how much of the variation in Table 5.6 should be attributed to this effect. For example, one source of variation may be the number of enzyme molecules adsorbed each time, and it is not clear how much this would be expected to change, since the scans are done in MMOH solution of equal concentration each time and the scan conditions do not change. It would be useful to obtain two separate calibration curves, under the same conditions, with the same adsorbed layer of enzyme. This may run into the limitation of how long the adsorbed layer remains active; for example, when the uteroferrin enzyme was contained within a thin film of surfactant, the electrochemical response became unstable a period of a few hours [10].

6.2 Comparison with Previous Works

One striking aspect of these results is that a relatively linear response was obtained by immobilizing MMOH alone. The work in [4] demonstrated that MMOR was not required, since the electron-supplying role of the reductase could also be fulfilled by the electrode. However, it is well documented that MMOB is necessary for the oxygenation reaction to occur, both in the natural system and the electrochemical one.

In the natural system, the role of MMOB is multi-faceted and not yet fully understood. It appears to regulate the oxygenation reaction by causing conformational changes in MMOH; earlier works showed that it led to increased product yield and rate of reaction (see Section 2.1). More recent work suggests that MMOB is necessary for the oxygenation reaction to occur at all; in the absence of the regulatory protein, oxygen is bound and reduced to water, and the intermediate that

reacts with methane does not form [19].

With this background in mind, the linear response to acetonitrile and methane can be interpreted in several ways. It is possible that electron transfer to the iron center is coupled with product formation, but in a relatively inefficient way; in this scenario, addition of MMOB to the system would allow more of the oxygenated product to form. An alternative situation, in which electron transfer leads to the reduction of oxygen instead of the formation of oxygenated product, is also possible. In other words, since MMOB is absent, product formation may not be occuring at all. If this were the case, the relationship between signal strength and substrate concentration would still have to be explained.

Kinetic studies have shown that substrate binding happens first, leading to the formation of a MMOH:methane complex [21]. While the catalytic cycle of MMOH shows oxygen binding to the active site before methane (Figure 2-2), these two results do not contradict each other. In the enzyme-substrate complex, methane is not bound at the active site, but rather in a hydrophobic pocket; it is then passed to the active site after the appropriate intermediates have been formed.

In one possible scenario, electron transfer to the active site then proceeds, in which the amount of electron transfer (and thus the intensity of current) depends on the amount of MMOH that has formed an enzyme-substrate complex. However, since MMOB is not present, the oxygenation reaction does not occur, and the reducing equivalents are used to reduce oxygen to water. If the concentration of oxygen is low relative to the substrate concentration, as is most likely the case in the degassed acetonitrile experiment, this may be a less plausible explanation. It is also not clear how the hydroxylase might regulate electron transfer so that only MMOH molecules bound to substrate receive electrons; this sort of regulation is quite likely, since it allows reducing equivalents to be used most efficiently, but in the full enzyme this effect is due to MMOB. Still, this hypothesis may provide a way to reconcile the experimental results obtained here with previous work which suggests that product formation cannot occur without the presence of MMOB.

The work of [4] found a noteworthy difference between the electrochemical system and the natural, NADH-driven one; in the electrochemical system, the presence of catalase was required for product formation, suggesting that H_2O_2 was being formed and then inactivating the enzyme. In fact, both catalase and MMOB were required for product formation. Our work shows that neither appears necessary for an electrical signal, proportional to substrate concentration, to be generated. This is not necessarily an inconsistency; as mentioned above, the presence of a substrate-dependent signal does not necessarily mean that product is being generated.

From the point of view of sensor development, the question of whether methanol is produced at the electrode may not be one of key importance. As long as the signal is related to methane concentration in a predictable, consistent way, the electrode can be used as a methane sensor, and the molecular and enzyme-level details are of secondary importance. However, in the sense that this work is a follow-up to [4], it would be desirable to confirm whether MMOB, catalase, or both are required for product formation. In [4], an experiment was conducted in which the electrode was held at reducing potentials for 30 minutes, and the oxygenated product was then detected by gas chromatography. Such an experiment would be useful to further explore the possibility of a MMOH-based methane sensor, as it would be very helpful to know why the substrate-dependent signal was being generated.

For comparison purposes, another key work is the graphite-pencil electrode experiment described in Chapter 3. That experiment is conceptually similar to ours; an electrode surface is modified by adsorption of a redox-active species that also acts as a catalyst, and then when an appropriate substrate is added to the system, a clear increase in current is observed. The results are more clear and easily interpreted in that case, though. When phosphomolybdic acid is adsorbed onto the pencil surface, the signal changes dramatically, with sharp peaks due to reversible multi-electron transfer. This is an example of the ideal case, in which there is a non-catalytic signal that can be used to calculate surface coverage.

With MMOH, though, the electron transfer may not be reversible; electrons can be transferred from the electrode to the active site, reducing Fe^{III} to Fe^{II}, but it is not clear if electron flow can proceed in the opposite direction. This may explain why only a reduction signal is observed for MMOH. Even on the reducing scan, though, an actual peak is not seen, since the current generally continues to increase until the switching potential is reached. For redox-active species in solution, peak formation is due to diffusion-limited mass transport (Chapter 3.1); for surface-adsorbed species, a peak is still seen, due to the finite amount of chemical on the surface. It is not clear why this sort of behavior is not observed for MMOH; however, a similar signal is also seen for cytochrome *c* peroxidase in the presence of H_2O_2 [24].

On the other hand, when the addition of H_2O_2 to the modified pencil electrode is compared to the addition of acetonitrile or methane in our work, the effect is similar. The catalytic reaction caused an increase in the reduction current; on the reverse scan, current was shifted towards more negative values as well (compare Figures 3-5 and 5-9). The main difference is that the MMOH signal became much broader as well; the difference in magnitude between reducing and oxidizing

Substrate	Data Points	R^2	K_m (μM)	i_{max} (μA)
CH_3CN	5	0.96	44	11.6
CH_4	6	0.96	252	5.9

Table 6.1: Michaelis-Menten constants for acetonitrile and methane

current increased with substrate concentration. It is not clear what causes this difference. As mentioned in Chapter 5, when scans are taken with MOPS-only blanks, this broad shape is also seen.

6.3 Theoretical Considerations

Cyclic voltammetry of an adsorbed enzyme is controlled by a three-step process involving transport of substrate from the bulk solution to the enzyme layer, the kinetics of the enzyme itself, and electron transfer from the electrode to the active site [24]. Substrate transport is controlled by diffusion, as described in Chapter 3, and is not affected by the adsorbed enzyme layer. The enzyme kinetics and electron transfer are specific to this type of system, though, and will be considered here.

In the Michaelis-Menten model of enzyme kinetics, the relationship between reaction rate and substrate concentration is described by v_{max}, the maximum reaction rate, and K_m, the substrate concentration at which reaction rate is half of the maximum. The equation can be expressed in the following form:

$$\frac{1}{v} = \frac{1}{v_{max}} + \frac{K_m}{v_{max}} \frac{1}{[S]} \tag{6.1}$$

where v is the reaction rate and [S] is the substrate concentration.

A plot of $1/v$ versus $1/[S]$, called a Lineweaver-Burk plot, allows values of K_m and i_{max} to be found from experimental data. Since the reaction rate v is proportional to current [6], Equation 6.1 is also valid for i and i_{max}. Michaelis-Menten constants were estimated for acetonitrile using the data in Figure 5-9 and for methane using the data in Figure 5-16. The results are shown in Figure 6-1 and summarized in Table 6.1.

According to the model, at substrate concentrations significantly lower than K_m, v is directly proportional to [S]; at concentrations significantly higher than K_m, v is independent of [S]. The lower value for acetonitrile reflects how the current (and charge transferred) no longer increases past about 80 μM, while for methane, no leveling-off was seen even around 900 μM. However, in other sets of methane data, the current stops increasing around 300 μM, so the K_m in that case

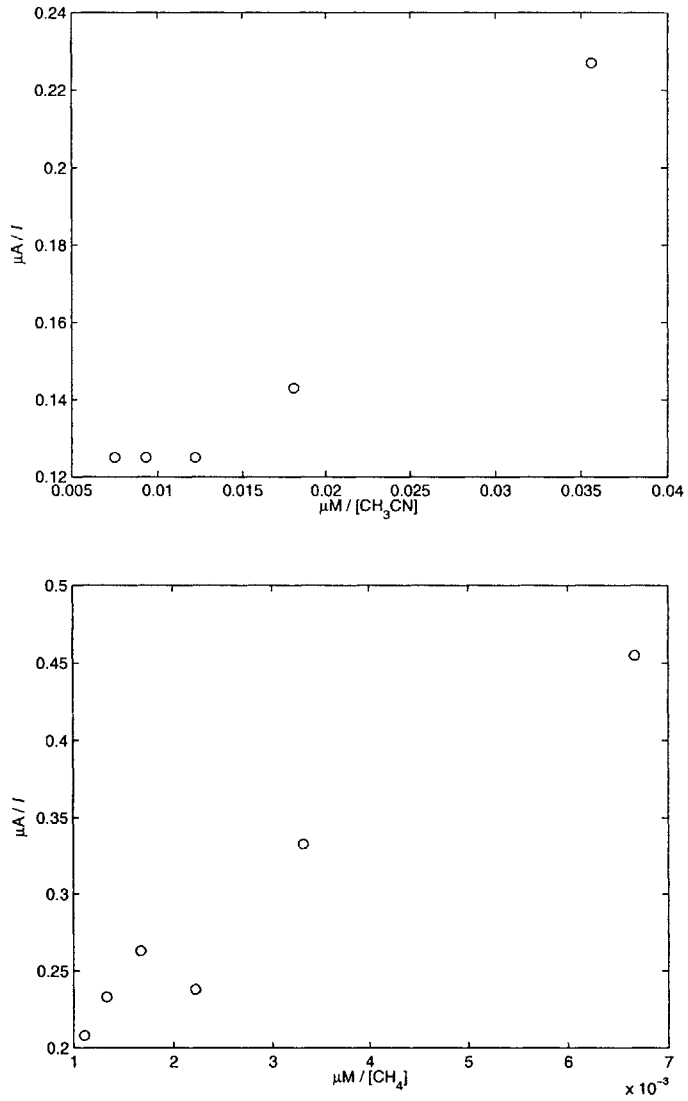

Figure 6-1: Lineweaver-Burk plots for acetonitrile and methane. For acetonitrile (top), the current in the plateau region was used; for methane (bottom), where no plateau region was consistently obvious, the peak current was used.

would be lower as well.

For enzymes with multiple substrates, the K_m for one substrate is dependent on concentrations of the other substrates. (In the natural system, these are O_2 and NADH.) Because the acetonitrile and methane experiments were done at different oxygen concentrations, it may not be that useful to compare the two values. Previous works estimated K_m for methane at 160 μM and 3 μM [21]; the lower estimate is probably more accurate, since it is based on purified protein rather than crude extract. A low K_m means the enzyme would be working at maximum speed in the presence of relatively low concentrations of substrate; from an ecological point of view, this would help methanotrophs survive under low-methane conditions.

If the 3 μM value of K_m is accurate for electrode-bound enzyme, it would also mean that current should not depend on $[CH_4]$ at the concentration ranges studied in this work. However, since only MMOH was immobilized, it is reasonable that the enzyme kinetics are different from when all components are present. Also, the act of immobilization can have a significant effect on the enzyme's affinity for substrate [13], further altering the value of K_m from that found in nature.

The electron-transfer model presented in Chapter 3 was also considered. In [4], the electron transfer rate k_{et} is found using the measured current, using the relationship $k_{et} = i/nFAC_o$, where n, F, and A are as defined in chapter 3 and C_o is the enzyme concentration in mol/cm^3. However, this relationship is not dimensionally correct; it leads to a k_{et} expressed in [L/T], rather than [T^{-1}]. If C_o is actually in mol/cm^2, and is estimated using the size of a MMOH molecule ($60 \times 100 \times 120$ Å, [46]) and the assumption of a close-packed monolayer, the resulting k_{et} is about 50 s^{-1}. However, k_{et} is reported in [4] as 3×10^{-5} s^{-1}.

Since it was not clear how to use our experimental data to back out a reasonable electron transfer rate, the one given in [4] was used to see if the electrochemistry data could be reconciled with what Marcus Theory predicts. It has been proposed that electron transfer to the active site occurs via the Tyr67 and Lys74 amino acids on the surface of the MMOH canyon, about 10 Å from the iron centers [46]. However, we assume that when MMOH is immobilized onto the electrode, the electrons need to be transferred over longer distances. This is because MMOB, the natural source of electrons (via NADH), can bind within the canyon; the flat electrode surface cannot come into such close contact.

If the distance is taken to be 30 Å instead, then Marcus Theory predicts an optimal electron transfer rate of about 9×10^{-4} s^{-1}. (Details of the calculation are as follows: The maximum rate, when the donor and acceptor molecules are in contact, is about 10^{13} s^{-1}. This is then adjusted

by the $\exp(-\beta(R - R_\circ))$ term in Equation 3.8, where $R_\circ = 3.6$ Å and $\beta = 1.4$ Å^{-1}; the value of β is appropriate for electron transfer through a protein [34].) This is an optimal rate because it does not consider the driving force or reorganizational energy (accounted for in Equation 3.9). The experimentally determined rate from [4] is about an order of magnitude lower, which seems reasonable; since the peak current values found in this work are similar to those in [4], we conclude that our data is in relatively good agreement with theoretical predictions of electron transfer rate.

Chapter 7

Conclusion

The work described in this thesis was based on the idea that we could take a current area of chemistry research and build on it for environmental sensing purposes. In the process, we answered some questions and raised many others. These current questions were mentioned throughout Chapter 5, and will be summarized here:

- Are methane and oxygen being stored by MMOH? Both the scan rate and oxygen-varying experiments showed clear differences in signal based on the order in which particular scans were recorded, and the most logical explanation is that the enzyme is storing substrates for later use.
- What is the effect of oxygen on the electrical response? For a given O_2 concentration, the signal could be partly dependent on oxygen being involved in the MMOH catalytic cycle, and also on oxygen being directly reduced (independently of MMOH) at the electrode surface.
- Can the signals produced during the control experiments be explained? In these experiments, the signal is not dependent on substrate concentration, as expected. However, the signals are nearly identical to those obtained when the MMOH-modified electrode is exposed to high concentrations of substrate.

The first question may be particularly important, as it relates to both microbial ecology and sensor design. Methanotrophs require both methane and oxygen, so they are abundant near the interface between oxygen-containing regions of water or sediment and oxygen-depleted, potentially methane-containing regions. Such an interface may shift with time, and if the methanotrophs can store one substrate for use when it is not present, this confers an ecological benefit. However, this

storage ability would also make it more difficult to design a methane sensor to reflect the current concentration of methane, rather than some complicated function of previous concentrations.

Contributions

This work made several contributions that can provide a useful building block for further research in the area of MMO-based methane sensors. For one thing, we found that a homemade instrumentation system can give useful results. This may sound trivial, but it allowed us to carry out interesting research without the purchase of expensive instrumentation, and may help others to do the same.

We have clearly shown that a MMOH-modified electrode responds to levels of substrate (acetonitrile or methane) and oxygen, and that the changing response is due to the presence of the enzyme. With acetonitrile, this response was linear within concentration limits, and we expect that methane would behave in a similar manner if more care were taken to prepare solutions of given concentration.

In typical cyclic voltammetry experiments, peak current is directly related to analyte concentration. We show that the charge transferred over a scan may be a more useful signal for use in sensors; throughout this work, the relationship between charge and concentration is closer to linear, and it also has the advantage of being taken over a time period, rather than instantaneously.

This work also suggests that a methane-sensing system may be effective with the hydroxylase (MMOH) component only, in contrast to previous works which concluded that at least the coupling protein (MMOB) was also required for product formation. As discussed in Chapter 5, our observation might not contradict the previous works, so much as explore the possibility that a reproducible electrical signal might be generated without formation of oxygenated product.

Limitations

As discussed throughout this thesis, several limitations have also become apparent over the course of this work. As mentioned in Chapter 6, the kinetics of gas-liquid partitioning were not properly accounted for in the methane experiments. It would be interesting to repeat some of the methane work using the headspace equilibration method of preparing solutions.

We currently do not have a good understanding of other sources of current in this system. Often, papers mention that background current has been subtracted, but it is not clear what causes the background signal. Dissolved oxygen is a possible culprit. Electrochemistry experiments typically

include a step of purging with inert gas to remove oxygen from the system as much as possible, since the oxygen signal can overwhelm other signals that are present. That could not be done in some of our trials, when we wanted O_2 to be present to investigate its effects on MMOH.

Also, if time had permitted, it would have been desirable to carry out the gas chromatography experiment described in Chapter 6, in which the electrode is held at negative potentials and oxygenated product is detected using gas chromatography. The experiment may be slightly complicated by the geometry of the gold electrode and small-volume cell, because the electrode must be removed from the cell in order to sample the solution, and the act of removal will mix the solution. It may be the case that enough product is formed that it can mix throughout the volume and still be detectable by a flame ionization detector, though.

Additional Ideas for Future Work

This work showed that electrical signal for a given concentration of methane also depended on the amount of oxygen present. As a result, for a MMO-based sensor to be effective, it needs to be demonstrated that there is a reproducible relationship between electrical signal and methane concentration, not just at 5 mg/L $[O_2]$ or another arbitrary level, but for a variety of oxygen levels.

Also, the effect of temperature, pressure, and ionic strength could be investigated. Most enzymes have a relatively narrow range of conditions that can be tolerated. The stability of MMOH, and its response to substrates, could be tested at a variety of conditions representative of what is found in natural waters.

In the end, while this work raises at least as many questions as it attempts to answer, hopefully it provides the beginnings of a framework for those who tackle the questions next.

Appendix A

Appendix

A.1 Potentiostat Circuit

The homebuilt potentiostat used in this project was developed by University of Wisconsin teaching staff based on a basic op amp potentiostat circuit in [50]. The potentiostat is used to drive the electrochemical system and measure its response; it maintains a certain voltage between the reference and working electrodes, and measures the resulting current that flows between the working and counter electrodes.

The circuit shown in Figure A-1 was constructed on a general-purpose breadboard and connected to a ±15-V power supply. Connections to the electrodes were made using alligator clips; the use of female pin connectors would also be appropriate. The electrode leads were twisted together and shielded to reduce stray noise pickup. All wires and resistors were cut to lie flat on the board surface, eliminating loops.

The original circuit produced an 0.7 V, 1 MHz oscillation when used for MOPS electrochemistry, though scans of $Fe(CN)_6$ in KCl were clean. A 0.05 μF capacitor was then connected between pins 2 and 3 of the OP27 in the loop between C and R. A low-pass filter was placed at V_{output}; instead of measuring at pin 6 directly, a 100K resistor and 0.2 μF capacitor were placed in series to ground, and the measurement was taken between the two. This resulted in a much cleaner signal, with noise of 5–10 mV.

An unrelated oscillation appears to be due to the placement of electrodes within the small-volume cell. This ±15 V, 20 KHz oscillation is usually present when the working and counter electrodes are placed in a given solution for the first time. An oscilloscope is used to monitor the output at the lead to the counter electrode. The counter electrode is removed from solution

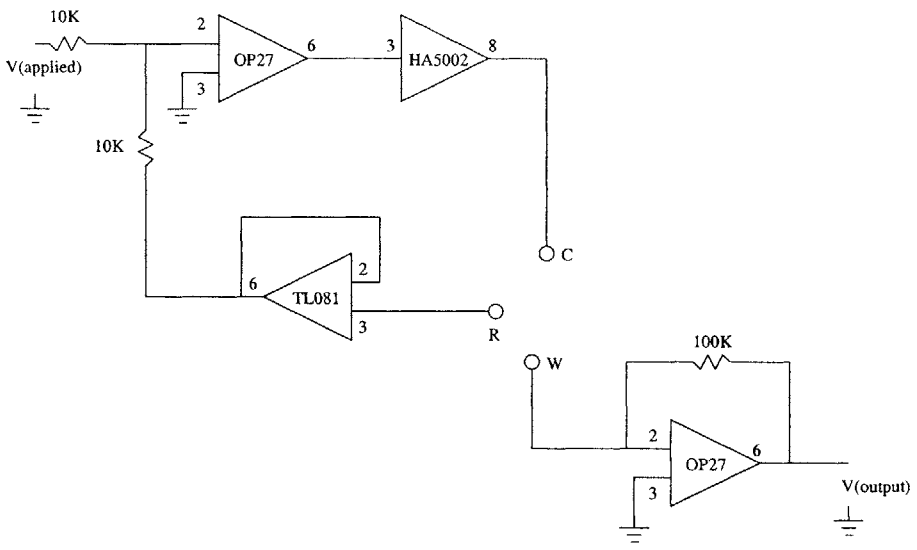

Figure A-1: Original potentiostat circuit diagram; see text for modifications.

and replaced until the oscilloscope trace is steady. When the starting or switching potentials are changed, the first subsequent scan often results in this ±15 V oscillation; in this case, the counter electrode must be adjusted, and the resulting data must be collected again.

A.2 LabVIEW Code

In the preliminary stage of this project, the triangle wave at $V_{applied}$ was controlled manually, using an analog circuit with an integrator and switch; V_{output} was recorded on a Perkin-Elmer 56 chart recorder. However, it soon became necessary to have both a more precisely controlled input and a way to record data numerically.

National Instruments' LabVIEW is a useful program for instrument control and data acquisition. It was installed on a Pentium III computer running Windows 2000. A PCI-6221 digital acquisition (DAQ) card was installed in the computer and connected to a SCB-68 shielded terminal block by a noise-rejecting, shielded cable (all from NI). Input and output leads, along with their respective ground lines, were connected to the terminal block.

The `potentiostat` program written to control $V_{applied}$ and record V_{output} is based in part on [20]; its block diagram, the graphical representation of code used in LabVIEW, is shown in Figure A-2. The program is referred to as a VI, or virtual instrument. On the front panel, which serves as the user interface and can contain controls similar to those of physical instruments, the user inputs the starting and switching potentials, the number of cycles, and the scan rate.

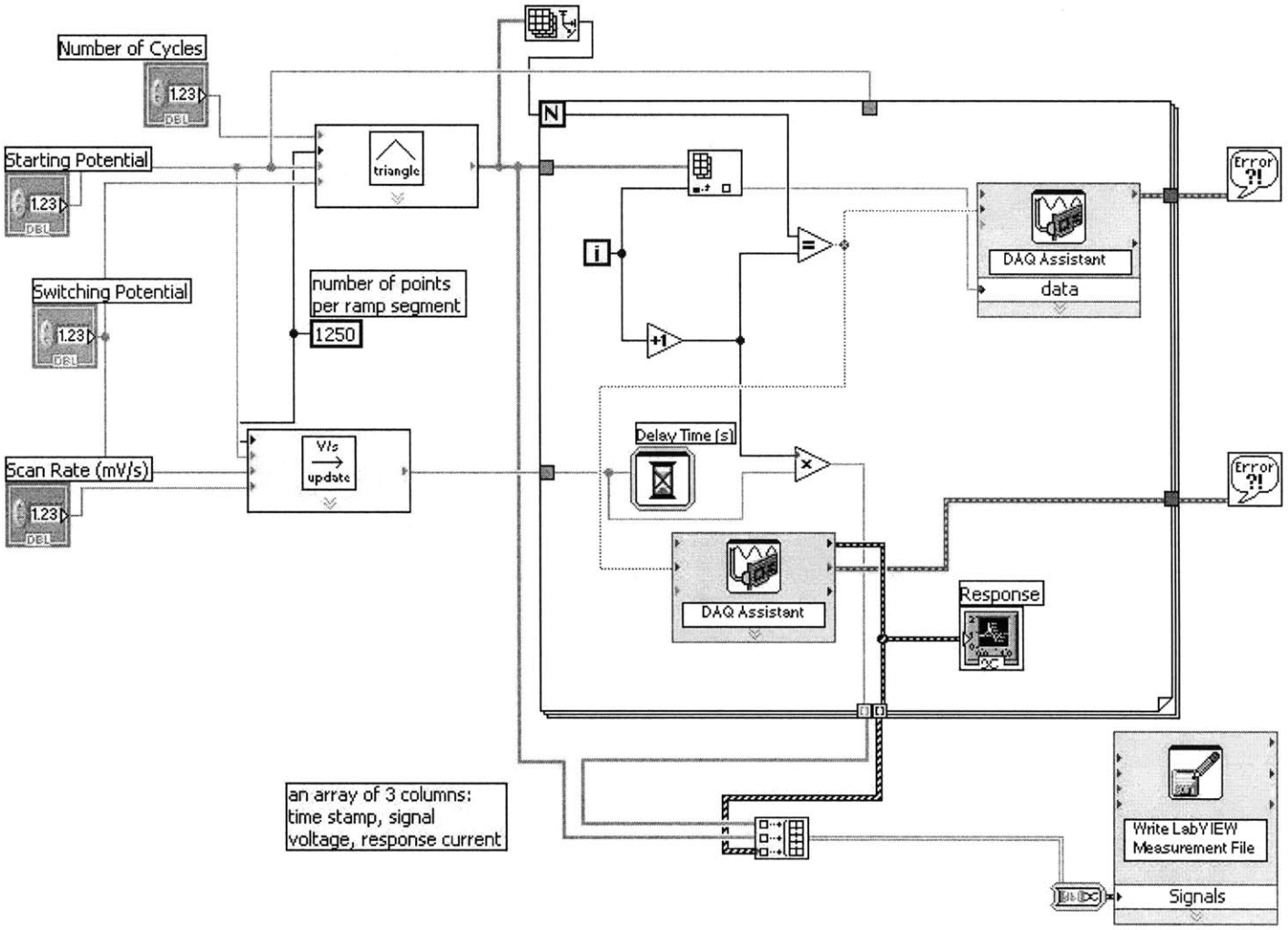

Figure A-2: Block diagram of overall `potentiostat` VI

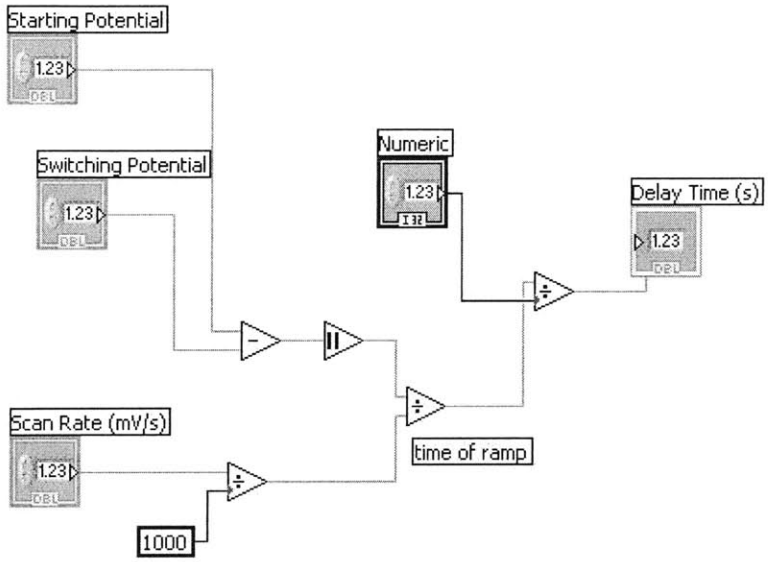

Figure A-3: Block diagram of `update` subVI

The block diagram contains two user-coded subVIs, or subprograms, labeled `update` and `triangle`. The `update` subVI, shown in Figure A-3, takes as inputs the starting and switching potentials and scan rate and calculates the total time of the ramp segment (one leg of the triangle wave). This is then divided by the number of data points collected per ramp segment to give a delay time, the time elapsed between data points. The `triangle` subVI, shown in Figure A-4, takes the starting and switching potentials, as well as the number of points in each segment, and uses predefined ramp functions to generate the applied voltage triangle wave (Figure 3-1). The code is enclosed in a For loop which executes n times, where n is the number of cycles; each time, the Build Array function appends the column to the previous result.

In the `potentiostat` program itself, most of the analog input/output code is enclosed in a For loop, which is indexed to the number of points in the triangle-wave array. With each iteration of the loop, the nth element in the array is extracted. The DAQ Assistant subVI, which is available within LabVIEW and can be modified for a particular task, takes this value and generates the required output voltage; this is $V_{applied}$ on the circuit diagram. Another DAQ Assistant subVI is set to record the input voltage from the i-V converter (this is V_{output} on the circuit diagram, but an input voltage to the data acquisition card). This value is also displayed on an indicator graph on the front panel. The DAQ Assistants generate or record one data point per iteration.

The delay time between iterations is set by the value computed by `update`. The DAQ Assistants are set to stop when the last element of the triangle-wave array has been extracted. A Simple Error

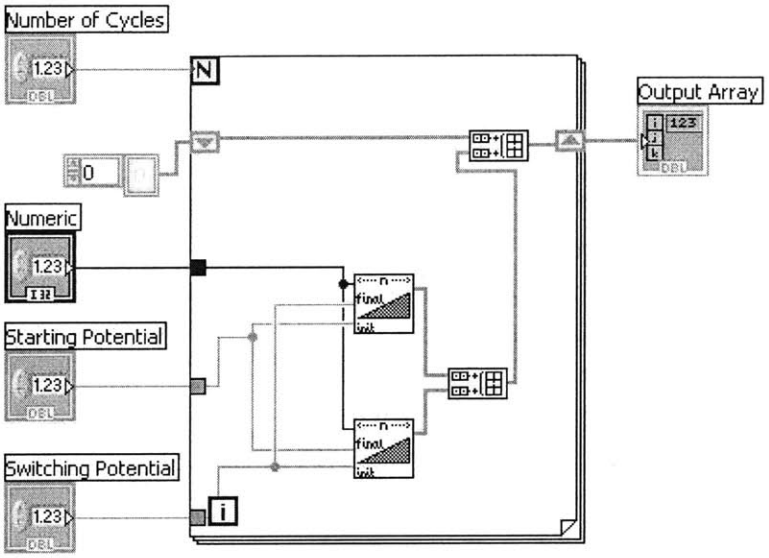

Figure A-4: Block diagram of `triangle` subVI

Handler is wired to each DAQ Assistant and placed outside the For loop.

Finally, the Build Array function is used to generate a matrix with columns corresponding to the time elapsed, the triangle-wave voltage points, and the measured voltage points. The latter two are passed out of the For loop using tunnels, which are set to append the value generated by the current iteration to the column of those generated previously. The Write LabVIEW Measurement File subVI, which like the DAQ Assistant is pre-defined and can be modified, writes the resulting matrix to a ASCII file and gives it a .lvm extension.

As shown here, the program records the V_{output} value. It would also be useful to divide by 100,000, the value of the resistor in the i-V converter, so that the current is recorded directly.

A.3 Matlab

The .lvm files can be conveniently processed using Matlab. The header portion of the file is deleted, leaving only the numerical values. The `load` function is used to store the matrix in the current workspace. The x-y plots characteristic of cyclic voltammetry are generated using the `plot` command:

```
> plot(filename(:,4),filename(:,6))
```

Columns 1, 3, and 5 of the .lvm file simply count each iteration of the For loop. Column 2 contains the time stamps. Columns 4 and 6 contain the voltage and current data; plotting current as a

function of applied voltage produces a cyclic voltammogram. Since there is still some noise in the signal, the `smooth` function can be applied to Column 6 to clean up the plot.

The plot can be modified with the `title`, `legend`, `xlabel`, and `ylabel` functions.

Since each data point is collected Δt apart, where Δt is set by the result of `update.vi`, the current can be integrated with respect to time (within a normalization factor) simply by adding each data point. It is useful to calculate total charge transferred for the forward and reverse scans separately, rather than for the total scan. This is done by extracting column vectors from the `filename` matrix:

```
> a = filename(1:1250,6)
> b = filename(1251:2500,6)
```

The number of data points per ramp segment, 1250 in this case, is set in the LabVIEW program. Finally, `sum(a,1)` and `sum(b,1)` are used to sum the values in each column.

The value of the peak current can be estimated from the x-y plot. Alternatively, `filename (1250,6)` returns the current at the switching potential. The use of `max` and `min` may also be useful, though the values returned will be slightly inflated due to noise.

Bibliography

[1] Peptide property calculator. www.basic.nwu.edu/biotools/ProteinCalc.html, accessed February 2005.

[2] Kristoffer K. Andersson, Wayne A. Froland, Sang-Kyu Lee, and John D. Lipscomb. Dioxygen independent oxygenation of hydrocarbons by methane monooxygenase hydroxylase component. *New Journal of Chemistry*, 15:411–415, 1991.

[3] Fraser A. Armstrong, H. Allen O. Hill, and Nicholas J. Walton. Direct electrochemistry of redox proteins. *Accounts of Chemical Research*, 21:407–413, 1988.

[4] Yann Astier, Suki Balendra, H. Allen O. Hill, Thomas J. Smith, and Howard Dalton. Cofactor-independent oxygenation reactions catalyzed by soluble methane monooxygenase at the surface of a modified gold electrode. *European Journal of Biochemistry*, 270:539–544, 2003.

[5] Suki Balendra, Claire Lesieur, Thomas J. Smith, and Howard Dalton. Positively charged amino acids are essential for electron transfer and protein-protein interactions in the soluble methane monooxygenase complex from *Methylococcus capsulatus* (Bath). *Biochemistry*, 41:2571–2579, 2002.

[6] Allen J. Bard and Larry R. Faulkner. *Electrochemical Methods: Fundamentals and Applications.* Wiley, 2nd edition, 2001.

[7] Paul D. Barker, Kati Di Gleria, H. Allen O. Hill, and Valerie J. Lowe. Electron transfer reactions of metalloproteins at peptide-modified gold electrodes. *European Journal of Biochemistry*, 190:171–175, 1990.

[8] Mekki Bayachou, Rong Lin, William Cho, and Patrick J. Farmer. Electrochemical reduction of NO by myoglobin in surfactant film: characterization and reactivity of the nitroxyl (NO^-) adduct. *Journal of the American Chemical Society*, 120:9888–9893, 1998.

[9] Elizabeth A. Bentley, Yann Astier, Wen Ming Ji, Stephen G. Bell, Luet-Lok Wong, and H. Allen O. Hill. The electrochemistry and scanning tunneling microscopy of the flavoprotein putidaredoxin reductase on alkanethiol-modified gold. *Inorganica Chimica Acta*, 356:343–348, 2003.

[10] Paul V. Bernhardt, Gerhard Schenk, and Gregory J. Wilson. Direct electrochemistry of porcine purple acid phosphatase (uteroferrin). *Biochemistry*, 43:10387–10392, 2004.

[11] Brian J. Brazeau, Bradley J. Wallar, and John D. Lipscomb. Effector proteins from $P450_{cam}$ and methane monooxygenase: lessons in tuning nature's powerful reagents. *Biochemical and Biophysical Research Communications*, 312:143–148, 2003.

[12] Anthony E. G. Cass, Graham Davis, Graeme D. Francis, H. Allen O. Hill, William J. Aston, I. John Higgins, Elliot V. Plotkin, Lesley D. L. Scott, and Anthony P. F. Turner. Ferrocene-mediated enzyme electrode for amperometric determination of glucose. *Analytical Chemistry*, 56:667–671, 1984.

[13] Hugh D. Conlon and David R. Walt. Immobilization of enzymes in polymer supports. *Journal of Chemical Education*, 63(4), 1986.

[14] Lars R. Damgaard, Niels Peter Revsbech, and Wolfgang Reichardt. Use of an oxygen-insensitive microscale biosensor for methane to measure methane concentration profiles in a rice paddy. *Applied and Environmental Microbiology*, 64(3):864–870, 1998.

[15] K. Di Gleria, H. A. O. Hill, V. J. Lowe, and D. J. Page. Direct electrochemistry of horse-heart cytochrome *c* at amino acid-modified gold electrodes. *Journal of Electroanalytical Chemistry*, 213, 1986.

[16] Nicola C. Foulds and Christopher R. Lowe. Immobilization of glucose oxidase in ferrocene-modified pyrrole polymers. *Analytical Chemistry*, 60:2473–2478, 1988.

[17] Jane E. Frew and H. Allen O. Hill. Direct and indirect electron transfer between electrodes and redox proteins. *European Journal of Biochemistry*, 172:261–269, 1988.

[18] Stephen C. Gallagher, Anastasia J. Callaghan, Jinkui Zhao, Howard Dalton, and Jill Trewhella. Global conformational changes control the reactivity of methane monooxygenase. *Biochemistry*, 38:6752–6760, 1999.

[19] George T. Gassner and Stephen J. Lippard. Component interactions in the soluble methane monooxygenase system from *Methylococcus capsulatus* (Bath). *Biochemistry*, 38:12768–12785, 1999.

[20] Rudy Gostowski. Teaching analytical instrument design with LabVIEW. *Journal of Chemical Education*, 73(12):1103–1107, 1996.

[21] Jeffrey Green and Harold Dalton. Steady-state kinetic analysis of soluble methane monooxygenase from *Methylococcus capsulatus* (Bath). *Biochemical Journal*, 236:155–162, 1986.

[22] Paul D. Hale, Leonid I. Boguslavsky, Toru Inagaki, Hiroko I. Karan, Hung Sui Lee, Terje A. Skotheim, and Yoshi Okamoto. Amperometric glucose biosensors based on redox polymer-mediated electron transfer. *Analytical Chemistry*, 63:677–682, 1991.

[23] Richard S. Hanson and Thomas E. Hanson. Methanotrophic bacteria. *Microbiological Reviews*, 60(2):439–471, 1996.

[24] Hendrik A. Heering, Judy Hirst, and Fraser A. Armstrong. Interpreting the cyclic voltammetry of electroactive enzymes adsorbed on electrodes. *Journal of Physical Chemistry B*, 102:6889–6902, 1998.

[25] Harold F. Hemond and Elizabeth J. Fechner-Levy. *Chemical Fate and Transport in the Environment.* Academic Press, 2nd edition, 2000.

[26] Michael L. Hitchman. *Measurement of Dissolved Oxygen*, volume 49 of *Chemical analysis.* Wiley-Interscience, 1978.

[27] Jeffrey A. Hurlbut, Thomas N. Ball, Harold C. Pound, and James L. Graves. Two convenient spectrophotometric enzyme assays. *Journal of Chemical Education*, 50(2), 1973.

[28] Yan Jiang, Patricia C. Wilkins, and Howard Dalton. Activation of the hydroxylase of sMMO from *Methylococcus capsulatus* (Bath) by hydrogen peroxide. *Biochimica et Biophysica Acta*, 1163, 1993.

[29] Eugenii Katz, Azalia Riklin, Vered Heleg-Shabtai, Itamar Willner, and A. F. Bückmann. Glucose oxidase electrodes via reconstitution of the apo-enzyme: tailoring of novel glucose biosensors. *Analytica Chimica Acta*, 385:45–58, 1999.

[30] Jurate Kazlauskaite, H. Allen O. Hill, Patricia C. Wilkins, and Howard Dalton. Direct electrochemistry of the hydroxylase of soluble methane monooxygenase from *Methylococcus capsulatus* (Bath). *European Journal of Biochemistry*, 241:552–556, 1996.

[31] Alexander M. Kilbanov. Immobilized enzymes and cells as practical catalysts. *Science*, 219:722–727, 1983.

[32] Peter T. Kissinger and William R. Heineman. Cyclic voltammetry. *Journal of Chemical Education*, 60(9):702–706, 1983.

[33] Raquel L. Lieberman, Deepak B. Shrestha, Peter E. Doan, Brian M. Hoffman, Timothy L. Stemmler, and Amy C. Rosenzweig. Purified particulate methane monooxygenase from *Methylococcus capsulatus* (Bath) is a dimer with both mononuclear copper and a copper-containing cluster. *Proceedings of the National Academy of Sciences*, 100(7):3820–3825, 2003.

[34] Stephen J. Lippard and Jeremy M. Berg. *Principles of Bioinorganic Chemistry.* University Science Books, 1994.

[35] John D. Lipscomb and Lawrence Que Jr. MMO: P450 in wolf's clothing? *Journal of Biological Inorganic Chemistry*, 3:331–336, 1998.

[36] Katherine E. Liu and Stephen J. Lippard. Studies of the soluble methane monooxygenase protein system: structure, component interactions, and hydroxylation mechanism. In *Advances in Inorganic Chemistry*, volume 42, pages 263–289. Academic Press, 1995.

[37] Gary A. Mabbott. An introduction to cyclic voltammetry. *Journal of Chemical Education*, 60(9):697–702, 1983.

[38] Asha Manoharan and Joseph H. Dreisbach. Applied enzymology. *Journal of Chemical Education*, 65(2):98–101, 1988.

[39] David Martel, Neso Sojic, and Alexander Kuhn. A simple student experiment for teaching surface electrochemistry: adsorption of polyoxometalate on graphite electrodes. *Journal of Chemical Education*, 79(3):349–352, 2002.

[40] Maarten Merkx, Daniel A. Kopp, Matthew H. Sazinsky, Jessica L. Blazyk, Jens Müller, and Stephen J. Lippard. Dioxygen activation and methane hydroxylation by soluble methane monooxygenase: a tale of two irons and three proteins. *Angewandte Chemie International Edition*, 40:2782–2807, 2001.

[41] R. Mukhopadhyay, K. K. Lo, L. L. Wong, and H. A. O. Hill. Oriented immobilization of *Pseudomonas putida* putidaredoxin at a gold(111)-buffer interface: a real time scanning tunnelling microscopy study. *Journal of Microscopy*, 213:6–10, 2004.

[42] Richard S. Nicholson and Irving Shain. Theory of stationary electrode polarography: single scan and cyclic methods applied to reversible, irreversible, and kinetic systems. *Analytical Chemistry*, 36(4):706–723, 1964.

[43] New Mexico State University Department of Chemistry and Biochemistry. (Alternative) experiment 4: Cyclic voltammetry. www.chemistry.nmsu.edu/studntres/chem435/Lab13, accessed February 2005.

[44] Thomas L. Riechel. A gas-sensor-based urea enzyme electrode. *Journal of Chemical Education*, 61(7), 1984.

[45] Azalia Riklin, Eugenil Katz, Itamar Willner, Achim Stocker, and Andreas F. Bückmann. Improving enzyme-electrode contacts by redox modification of cofactors. *Nature*, 376:672–675, 1995.

[46] Amy C. Rosenzweig, Christin A. Frederick, Stephen J. Lippard, and Pär Nordlund. Crystal structure of a bacterial non-haem iron hydroxylase that catalyzes the biological oxidation of methane. *Nature*, 366, 1993.

[47] Donald T. Sawyer, Andrzej Sobkowiak, and Julian L. Roberts Jr. *Electrochemistry for Chemists*. Wiley, 2nd edition, 1995.

[48] Rene P. Schwarzenbach, Philip M. Gschwend, and Dieter M. Imboden. *Environmental Organic Chemistry*. Wiley-Interscience, 2nd edition, 2003.

[49] G. Sittampalam and G. S. Wilson. Amperometric determination of glucose at parts per million levels with immobilized glucose oxidase. *Journal of Chemical Education*, 59(1):70–73, 1982.

[50] Douglas A. Skoog, Donald M. West, and F. James Holler. *Fundamentals of Analytical Chemistry*. Saunders, 7th edition, 1996.

[51] Shannon S. Stahl, Wilson A. Francisco, Maarten Merkx, Judith P. Klinman, and Stephen J. Lippard. Oxygen kinetic isotope effects in soluble methane monooxygenase. *Journal of Biological Chemistry*, 276(7):4549–4553, 2001.

[52] Medical Device Technology. Biosensors: a brief tutorial. www.fraserclan.com/biosens2.htm, accessed September 2003, 1994.

[53] Bradley J. Wallar and John D. Lipscomb. Methane monooxygenase component B mutants alter the kinetics of steps throughout the catalytic cycle. *Biochemistry*, 40, 2001.

[54] Douglas A. Whittington and Stephen J. Lippard. Methane monooxygenase hydroxylase. In Albrecht Messerschmidt, editor, *Handbook of Metalloproteins*, pages 712–724. Wiley, 2001.